
Deep Learning for Stable Monotone Dynamical Systems

Yu Wang, Qitong Gao, and Miroslav Pajic

Electrical and Computer Engineering

Duke University, Durham NC, USA

{yu.wang094,qitong.gao,miroslav.pajic}@duke.edu

Abstract

Monotone systems, originating from real-world (e.g., biological or chemical) applications, are a class of dynamical systems that preserves a partial order of system states over time. In this work, we introduce a feedforward neural networks (FNNs)-based method to learn the dynamics of unknown stable nonlinear monotone systems. We propose the use of nonnegative neural networks and batch normalization, which in general enables the FNNs to capture the monotonicity conditions without reducing the expressiveness. To concurrently ensure stability during training, we adopt an alternating learning method to simultaneously learn the system dynamics and corresponding Lyapunov function, while exploiting monotonicity of the system. The combination of the monotonicity and stability constraints ensures that the learned dynamics preserves both properties, while significantly reducing learning errors. Finally, our techniques are evaluated on two complex biological and chemical systems.

1 Introduction

Monotonicity is an important property of many complex dynamical systems [1], such as traffic networks [2], chemical reactions [3], and bio-ecological models [4]. A monotone dynamical system preserves a partial order of the system states; i.e., the state at the next time should increase if the state at current time has increased, as illustrated in Figure 1 for two evolutions of a monotone system where the initial state of $x'(t)$ path (i.e., $x'(0)$) is larger than $x(0)$. For example, in a bio-ecological model of several cooperative species, if we increase the population of one specie at some time (e.g., by bringing in new ones from outside), then the population of other species should increase afterwards.

In practice, these monotone models are usually nonlinear and unknown, so identifying them using classical approaches is difficult. Recently, there is a growing effort in using neural networks (NNs) to study the behavior of unknown nonlinear dynamical systems. For example, NNs are used to learn the (non-convex) control Lyapunov functions of the systems from samples [5, 6].

In this work, we use NNs to directly learn a model of an autonomous discrete-time system with unknown but monotone (non-decreasing) and stable dynamics

$$x(t+1) = f(x(t)); \quad (1)$$

here, $t \in \mathbb{N}$ is the *time*, $x \in \mathbb{R}^n$ denotes the *system state*, and f is a Lipschitz continuous nonlinear function. The dynamics of the system (1) is *monotone* in the sense that for any states x and y , if x is greater y entry-wise, then $f(x)$ is greater $f(y)$ entry-wise.

To learn the dynamics (1), we adopt a q -window approach for prediction; specifically, we train a network \hat{f} to predict the next system state from a q -window of past states – i.e., $x(t+1) =$

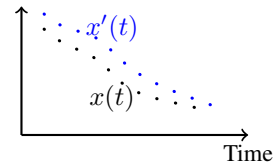


Figure 1: Paths of monotone systems.

$\hat{f}(x(t), x(t-1), \dots, x(t-q+1))$ (Section 3.1). Unlike the single step approach of predicting $x(t+1)$ from $x(t)$, the q -window prediction exploits the dependencies of $x(t+1)$ to $x(t), \dots, x(t-q+1)$, and thus, can be more accurate. In addition, to ensure monotonicity of the learned dynamics, we introduce a weight-based methods using feed-forward neural networks (FNNs) (Section 3.2). The weight-based method is designed for the FNN to capture monotonicity conditions in general without reducing its representation power; this is achieved through a fusion of nonnegative neural networks and batch normalization (BN). Finally, to control the learning error for long time-horizons, we impose the stability constraint on the learned dynamics. This is done by simultaneously learning the dynamics and its Lyapunov function through alternately minimizing the loss functions that combines the mean-square errors on the samples paths and the Lyapunov conditions (Section 3.3).

Our overall learning approach is illustrated in Figure 2.

The dynamics is learned by an FNN \hat{f} using the combination of sample paths, the monotonicity condition, and the Lyapunov condition; the Lyapunov function of \hat{f} is learned by another FNN \hat{V} using the Lyapunov condition.

We evaluate our methods to impose monotonicity and stability constraints on two case studies (Section 4): (1) the

Lotka-Volterra model of two cooperative species that can migrate between multiple patches, and (2) the biochemical control circuit of the translation from DNA to mRNA. Our results show that imposing the stability and monotonicity constraints ensures the stability of the learned FNN, as well as the monotonicity at most test points. In addition, the approximation error of the FNN \hat{f} to the system f from (1) is significantly reduced, especially for long time-horizons.

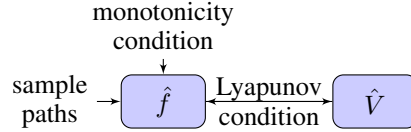


Figure 2: Diagram of learning setup

Related Work. Imposing monotonicity constraints in learning originates from classification and regression of data whose labels increase (or decrease) with the features (e.g., the dependence of the value of a used car on its mileage). To handle such data, monotonicity constraints were imposed for kernel machines [7] and trees [8, 9]. The focus of this work is to allow for imposing monotonicity constraints to learning dynamical systems.

One method to impose monotonicity focuses on the structure and weights of the NNs. For example, it is proposed to set single weights to be positive [10] for certain classification problems or introduce constraints between multiple weights [11, 9, 12]. Alternatively, specific NN structures are introduced, from a simple three-layer NN [13] to a more complex structure combining linear calibrators and lattices [14]. On the other hand, to enable capturing general nonlinear functions, we propose to use two-layer NNs with both min-ReLU and max-ReLU activation functions with nonnegative weights. In addition, to avoid sub-optimal outcomes [15] due to the hard constraints in training, we employ batch normalization to ‘soften’ the constraints; this enables stochastic gradient-based optimizers to jointly balance among multiple learning objectives in each training step. In our case studies, we show that combination of these two methods can accurately approximate system dynamics, without significantly affecting monotonicity conditions.

Another approach is to impose monotonicity as a penalty to the training loss, computed for a set of samples [16] or the average of some pre-defined distribution [17]; hence, monotonicity is only imposed for that set of samples or distribution. On the other hand, our weight-based method does not depend on the choice of the samples or distribution. In addition, most of the aforementioned works [10, 13, 18, 14, 11] focus on NNs with categorical outputs, while we focus on dynamical systems, where system outputs are real vectors. Finally, a monotone function could also be indirectly obtained by learning its derivative using an NN that only provides nonnegative outputs [19]. However, recovering the monotone function from the trained NN would require integration; thus, any learning errors would accumulate over the integration/time, effectively resulting in large approximation errors.

In this work, inspired by the common idea of using piecewise linear dynamics to approximate (known) nonlinear dynamics in non-learning context [20, 18], we consider a NN with ReLU activation functions (instead of sigmoid). Similar to [13, 11], our NN can be viewed as a piecewise linear approximation of a nonlinear function; its monotonicity achieved by enforcing positive weights. However, our ReLU NN is more versatile, and can have any number of layers, which is needed to enable learning for complex nonlinear dynamical systems, beyond classification and regression [21].

Compared to existing work on learning for Lyapunov functions [5, 6], we simultaneously learn the unknown dynamics and its Lyapunov function, which is similar in spirit to the idea from [22].

However, our update rule for learning the dynamics is different, as the method from [22] does not apply to q -window prediction. Specifically, instead of projecting the dynamics against the learned Lyapunov function [22] to keep them consistent with respect to the Lyapunov condition, we propose to penalize the inconsistency between the learned dynamics and Lyapunov function during learning. This technique is compatible with our q -window prediction approach.

2 Preliminaries

We consider the problem of training an NN to approximate the dynamics of an unknown discrete-time monotonically non-decreasing and stable system (1), by training from sample system trajectories. We first formally introduce such systems as follows.

For a given initial state, we refer to the corresponding solution $x(t)$ of (1) as a *trajectory* of the system. The system (1) is a *monotone* system, if it preserves some partial order \preceq on \mathbb{R}^n . In this work, we consider a common partial order [1] defined as

$$x \preceq y \iff x_i \leq y_i \text{ for all } i \in [n], \quad (2)$$

where $[n] = \{1, \dots, n\}$, $x, y \in \mathbb{R}^n$, and $x_i, y_i \in \mathbb{R}$ denote their i -th entry.

Monotone systems. The system (1) is *monotone* on domain $D \subseteq \mathbb{R}^n$ if for any two trajectories $x_1(t), x_2(t) \in D$, it holds that

$$x_1(0) \preceq x_2(0) \implies x_1(t) \preceq x_2(t) \text{ for all } t \in \mathbb{N}. \quad (3)$$

The system (1) is *monotone* if and only if the function f is monotonically non-decreasing in the common sense – i.e., if for any two inputs $x_1, x_2 \in \mathbb{R}^n$, it holds that $x_1 \preceq x_2 \implies f(x_1) \preceq f(x_2)$.

Example 1. A scalar linear system $x(t+1) = ax(t)$ is monotone on the domain $[0, +\infty)$ for any $a \geq 0$, since for any two initial states $x_1(0) \leq x_2(0)$, the two corresponding trajectories satisfy $x_1(t) = a^t x_1(0) \leq a^t x_2(0) = x_2(t)$. Therefore, the ordering between the initial states is preserved during the evolution of two trajectories for all times $t \in \mathbb{N}$.

It is important to highlight that the monotonicity is defined for the (initial) state not for the time, as illustrated in Figure 1. From Example 1, when $a \in (0, 1)$, the trajectory $x(t) = a^t x(0)$ decreases with the time t ; yet, the system is still monotone with respect to the initial state $x(0)$.

The monotonicity of the system (1) can be equivalently characterized by the gradient of function $f(x)$, as captured in the following lemma from.

Lemma 1. [1] The system (1) is monotone if and only if $\frac{\partial f}{\partial x_i} \geq 0$ for each entry x_i , ($i = 1, \dots, n$) of $x \in \mathbb{R}^n$. Specially, if the system (1) is linear – i.e., $f(x) = Ax$ for some $A \in \mathbb{R}^{n \times n}$, then it is monotone if and only if each entry A_{ij} , ($i, j \in [n]$) of the matrix A satisfies that $A_{ij} \geq 0$.

Lyapunov functions. The system (1) is *globally asymptotically stable* (or *stable* for short), if and only if it has a (discrete-time) Lyapunov function $V(x)$ [23]. Suppose that $x = 0$ is the stable point of the system (i.e., $f(0) = 0$) in general, a stable point x_0 can be moved to 0 by substituting x with $x - x_0$ in the system (1). Then $V(x)$ should satisfy the *Lyapunov condition* that

$$V(0) = 0, \quad \text{and } \forall x \neq 0, V(x) > 0, \quad \text{and } V(f(x)) - V(x) < 0. \quad (4)$$

The Lyapunov function can be viewed as a ‘potential’ with zero value at the stable point and positive values elsewhere. For stable systems, since the *discrete Lie derivative* $V(f(x)) - V(x)$ is negative, the (positive) value of the Lyapunov function should decrease along the system path so that it finally converges to zero at the stable point. For monotone stable systems, the Lyapunov function can always be written as the maximum of scalar functions [1] – there exist scalar functions $V_i : \mathbb{R} \rightarrow \mathbb{R}$ such that

$$V(x) = \max_{i \in [n]} V_i(x_i), \quad \text{for } [n] = \{1, \dots, n\}. \quad (5)$$

(5) provides a foundation of our technique to efficiently learn Lyapunov function of \hat{f} by an NN \hat{V} .

3 Monotone Neural Network

In this work, we introduce a window-based method to utilize FNNs to learn the dynamics of the system (1). We first show that this method can reduce the learning error in general (Section 3.1), as well as how to impose the monotonicity and stability constraints (Sections 3.2 and 3.3, respectively).

3.1 Window-Based Learning Method

Conventionally (e.g., [5, 6, 22]), to learn the dynamics f of the system (1), an FNN \hat{f}_γ with the weights γ may be trained to predict the next state $x(t+1)$ from the current state $x(t)$. Thus, to predict a future $x(t+T)$ from the state $x(t)$, the T -fold composition $\hat{f}_\gamma^{(T)}(x(t)) = \underbrace{\hat{f}_\gamma(\hat{f}_\gamma(\cdots \hat{f}_\gamma(\cdot)))}_{T \text{ in total}}$

of \hat{f}_γ can be used. In that case, the prediction error is captured by the following lemma.

Lemma 2. *Let us assume that (i) $\exists a, b \in \mathbb{R}$ s.t. $a\|x_1 - x_2\| \leq \|f(x_1) - f(x_2)\| \leq b\|x_1 - x_2\|$ and $a\|x_1 - x_2\| \leq \|\hat{f}_\gamma(x_1) - \hat{f}_\gamma(x_2)\| \leq b\|x_1 - x_2\|$ for all $x_1, x_2 \in \mathbb{R}^n$; and (ii) each element in the one step estimation error vector $\delta_\gamma(x(t+i-1)) = f(x(t+i-1)) - \hat{f}_\gamma(x(t+i-1))$ distributes uniformly in $[-\varepsilon, \varepsilon]$ for all $i \in [1, T]$. Then, an approximate lower bound of variance of each element in $x(t+T) - \hat{f}_\gamma^{(T)}(x(t))$ when iteratively predicting $x(t+T)$ from $x(t)$ is $(\sum_{i=1}^T a^{2(i-1)})\varepsilon^2/3$.*

Assumption (i) captures that f is a Lipschitz function and \hat{f}_γ in general captures the gradient properties of f . Assumption (ii) refers to a similar case analyzed in [24], which implies if an \hat{f}_γ is trained with stochastic gradient-based algorithms on same training data sufficiently large number of times (each time is with a unique initialization), then all predictions are assumed to be centered at the corresponding ground truth value with some disturbance bounded by ε .

The proof of Lemma 2 can be found in Appendix A.1. Note that, from the lemma, for $a > 1$ (i.e., when the system is unstable), the accumulated variance increases exponentially with respect to T .

To reduce the prediction error, we propose to train a set of FNNs $\mathcal{F}_\theta = \{\hat{f}_{\theta_i} \mid i = 1, \dots, q\}$ using a q -window of previous states $x(t:t-q+1) = (x(t), \dots, x(t-q+1))$, i.e., \mathcal{F}_θ predicts $x(t+1)$ from $x(t:t-q+1)$, where θ_i refers to the weights of the i^{th} estimator in \mathcal{F}_θ and θ represents all the parameters in \mathcal{F}_θ in general. Specifically, we can rewrite (1) as

$$x(t+1) = p_1 f(x(t)) + p_2 f^{(2)}(x(t-1)) + \cdots + p_q f^{(q)}(x(t-q+1)), \quad (6)$$

where q is the window length and $\sum_{i=1}^q p_i = 1$. Then $x(t+1)$ can be approximated by \mathcal{F}_θ as

$$\hat{x}(t+1) = p_1 \hat{f}_{\theta_1}(x(t)) + p_2 \hat{f}_{\theta_2}(x(t-1)) + \cdots + p_q \hat{f}_{\theta_q}(x(t-q+1)), \quad (7)$$

where $\sum_{i=1}^q p_i = 1$, $p_i \geq 0$, and ideally after training each \hat{f}_{θ_i} predicts $f^{(i)}(x)$ from x . In this case, all the θ_i 's can be obtained by solving the following optimization problem with a dual objective – i.e.,

$$\min_{\theta_i, p_i} \mathbb{E}_{x(\cdot) \sim \rho} [\|x(t+1) - \sum_{i=1}^q p_i \hat{f}_{\theta_i}(x(t-i+1))\|^2] \quad \text{s.t.} \quad \sum_{i=1}^q p_i = 1, \text{ and } p_i > 0; \quad (8)$$

here, ρ is the state visitation distribution from a random initial state $x(0)$, $t \in \{0, \dots, H\}$ and H is the system time horizon. In general, (8) can be achieved by either solving the corresponding primal-dual problem, or a two-step method which starts with training \hat{f}_{θ_i} 's separately followed by solving the linear programming problem w.r.t p_i 's. Note that given $x(t:t-q+1)$, we can estimate $x(t+T)$ using recursion as shown in Appendix E Alg. 1. In the following theorem we show that if a set of FNNs \mathcal{F}_θ is trained using (8), then the variance of approximation error is upper bounded.

Theorem 1. *Let us assume that: (i) there exists $0 < \eta \ll 1$ such that $\forall i \in \{1, \dots, q\}$, $|p_i - 1/q| \leq \eta$; (ii) $\exists a, b$ s.t. $a\|x_1 - x_2\| \leq \|f(x_1) - f(x_2)\| \leq b\|x_1 - x_2\|$ and $a\|x_1 - x_2\| \leq \|\hat{f}_{\theta_i}(x_1) - \hat{f}_{\theta_i}(x_2)\| \leq b\|x_1 - x_2\| \forall i \in \{1, \dots, q\}$; (iii) $b^k/q^k \approx 0$ for all $k \geq 4$; and (iv) each element in the error vector $\delta_{\theta_i}(x(t-i+1)) = \hat{f}_{\theta_i}(x(t-i+1)) - f^{(i)}(x(t-i+1))$ distributes uniformly in $[-\varepsilon, \varepsilon]$ for all $i \in \{1, \dots, q\}$. If \mathcal{F}_θ is trained using (8), the variance of each element in $x(t+T) - \hat{x}(t+T)$ when iteratively predicting $x(t+T)$ using q -window is approximately upper bounded by $(1 + \frac{b^2 + \varepsilon^2/3}{q}) \frac{\varepsilon^2}{3q}$.*

Theorem 1 proof and rationale of assumptions are provided in Appendix A, whereas the relatively strong condition (i) is, for the analyzed systems (from Section 4), numerically verified to hold in Appendix C. Note that the error bound from Theorem 1 does not increase with T ; this is also numerically validated in Section 4 for ($q = 100$)-window learning. From Lemma 2 and Theorem 1, the variance of estimating $x(t+T)$ using the q -window approach (7) is upper bounded by the recursive prediction $\hat{f}_\gamma^{(T)}(x(t))$ when it holds that

$$(q + b^2 + \varepsilon^2/3)/q^2 \leq \left(\sum_{i=1}^T a^{2(i-1)}\right). \quad (9)$$

Note that (9) may not always hold in general; and we analyze two nonlinear systems in Section 4, where one (9) satisfies and the other does not. However, in Section 4, we show numerically that even when (9) is not satisfied, the prediction error using q -window learning does not increase significantly compared to the error of $\hat{f}_\gamma^{(T)}(x(t))$.

Practically, when approximating $x(t+1)$, we can introduce a bias term b into (7) – i.e.,

$$\hat{x}(t+1) = p_1 \hat{f}_{\theta_1}(x(t)) + p_2 \hat{f}_{\theta_2}(x(t-1)) + \dots + p_q \hat{f}_{\theta_q}(x(t-q+1)) + z. \quad (10)$$

Since all the estimators in \mathcal{F} are FNNs, the p_i 's and z in the right side of (10) can be interpreted as the weights of a fully connected layer (with bias term added) that takes as input the output of all the estimators in \mathcal{F} . Thus, all the parameters can be encapsulated into a meta-NN \hat{f}_θ with weights θ , as¹

$$\hat{x}(t+1) = \hat{f}_\theta(x(t), x(t-1), \dots, x(t-q+1)), \quad (11)$$

which can be trained by minimizing the loss

$$\mathbb{E}_{x(\cdot) \sim \rho} [\|x(t+1) - \hat{f}_\theta(x(t), x(t-1), \dots, x(t-q+1))\|^2]. \quad (12)$$

In practice, the expectation in loss (12) is substituted by the empirical training loss for a batch of N given sample paths of the time horizon H , i.e.,

$$J(\hat{f}_\theta) = \frac{1}{N} \sum_{i=1}^N \frac{1}{H-q-1} \sum_{t=q-1}^{H-1} \|x_i(t+1) - \hat{f}_\theta(x_i(t), x_i(t-1), \dots, x_i(t-q+1))\|^2, \quad (13)$$

where N is the batch size and $x_i(\cdot)$ represents the state obtained from the i^{th} sample path for all $i \in \{1, \dots, N\}$. Note that \hat{f}_θ can be used to predict $x(t+T)$ given $x(t : t-q+1)$ by slightly modifying the recursion function in Appendix E Alg. 1, which in turn results in Appendix E Alg. 2.

3.2 Imposing the Monotonicity Constraint

Our method requires the input-output relation of each neuron to be monotone so that the overall input-output relation of the FNN is monotone. This is done by setting the weights in the FNN to be nonnegative. This can be achieved by resetting the negative weights to zero, or to relatively small random numbers that are close to zero, after each back propagation operation, as in the Dropout [25] method that prevents deep neural networks from overfitting. We refer to such NNs as *nonnegative NNs*.

We use the following rectified linear unit (ReLU) activation functions

$$\varphi(x_1, \dots, x_d) = \max \left\{ \sum_{i \in [d]} \theta_i x_i + \theta_0, 0 \right\} \text{ or } \min \left\{ \sum_{i \in [d]} \theta_i x_i + \theta_0, 0 \right\}, \quad \theta_1, \dots, \theta_d \geq 0, \quad (14)$$

where $x_1, \dots, x_d \in \mathbb{R}$ are the inputs to the neurons, θ_0 is the bias, and $\theta_1, \dots, \theta_d$ are the weights of the inputs. This is inspired by the use, in non-learning context, of piecewise linear dynamics to approximate known nonlinear dynamics [20, 18]. Specifically, as φ is a piecewise linear function, the FNN \hat{f}_θ using such activation functions is also piecewise linear. Thus, it can serve as a piecewise linear approximation, if trained to approximate the dynamics (1). Finally, the min-ReLU activations in (14) are needed to allow for capturing general nonlinear dynamics, due to the following claim (see Appendix A.3 for proof).

Claim 1. *If an FNN \hat{f}_θ only has the max-ReLU activations from (14), then \hat{f}_θ is convex.*

Since the activations from (14) are monotone, the following holds (see Appendix A.4 for the proof).

Theorem 2. *An FNN using the activations from (14) is monotone.*

We note that the inverse of Theorem 2 may not be necessarily true; i.e., a monotone NN can have negative weights. For example, consider an NN with two hidden layers, each containing a single-neuron. The output of the first hidden layer is $y_1 = \max\{x_1, 1\}$ given its input x_1 . The ReLU activation in the second hidden layer with a negative weight, computes $z_1 = \max\{-y_1, 1\}$ from the output of the first neuron y_1 . Yet, the NN is still monotone as the output is always 1. In addition, the dynamics represented by a monotone NN may decrease over time. For example, consider the single-neuron network that computes $x_1(t+1) = \max\{0.5x_1(t), 1\}$ from the input $x_1(t)$. For an initial state $x_1(0) = 10$, the corresponding trajectory is decreasing with time $t \in \mathbb{N}$.

¹Without loss of generality, we slightly abuse θ here, as well as in the rest of the paper, to represent the weights within the meta-NN instead of referring to all the parameters in \mathcal{F} in general as in (7).

Batch Normalization. Generally, imposing hard constraints on the weights can lead to undesirable sub-optimal results in training, as observed in [15]. Hence, instead of straightly imposing the positive weight constraint $\theta_0, \dots, \theta_d \geq 0$ for the activations (14), we propose to use batch normalization (BN) [26] to soften the constraints and ensure the representation power of \hat{f}_θ . This is because the BN parameters are allowed to converge to optima defined in a broader search space if necessary, but can be trained to satisfy the weight constraints as well if it is optimal to do so; although this may lead to tolerable (minor) violations of the hard constraints, as we show in the applications in Section 4.

3.3 Imposing the Stability Constraint

When the system (1) of interest is stable, we introduce the following *alternating* learning [27] method to ensure stability of the trained FNN. Recall that the system is stable if and only if it has a Lyapunov function $V(x)$ in the form of (5); in our case the goal is to have $V(x)$ also represented by an FNN $\hat{V}_\xi(x)$. We employ an optimization framework [27] that learns \hat{f}_θ and \hat{V}_ξ simultaneously in each epoch by alternately minimizing the training loss for each estimator alternately. Specifically, to train \hat{f}_θ , we impose the Lyapunov condition (4) by minimizing the following *expected* loss for violating the Lyapunov condition

$$\min_{\xi} \mathbb{E}_{x(\cdot) \sim \rho} \left(\hat{V}_\xi(0)^2 + [-\hat{V}_\xi(x(t))]^+ + [\hat{V}_\xi(\hat{f}_\theta(x(t : t - q + 1))) - \hat{V}_\xi(x(t))]^+ \right), \quad (15)$$

where the expectation $\mathbb{E}_{x(\cdot) \sim \rho}$ follows from (8). In (15), the first term penalizes the non-zero value of $\hat{V}_\xi(0)$, the second term penalizes the negative values of $\hat{V}_\xi(x)$, and the third term penalizes the positive values of the discrete Lie derivative of \hat{V}_ξ for \hat{f}_θ , as discussed in Section 2. Effectively, our approach can be viewed as a discrete-time version of the training loss for the Lyapunov function from [6].

In practice, the expected loss of (15) is approximated by the average of N sample paths of length $H \gg q$ - i.e., to impose the Lyapunov condition, while training FNN \hat{V}_ξ , we utilize the loss function

$$\min_{\xi} \frac{1}{N} \sum_{i=1}^N \frac{1}{H - q - 1} \sum_{t=q-1}^{H-1} \left(\hat{V}_\xi(0)^2 + [-\hat{V}_\xi(x_i(t))]^+ + [\hat{V}_\xi(\hat{f}_\theta(x_i(t : t - q + 1))) - \hat{V}_\xi(x_i(t))]^+ \right). \quad (16)$$

Finally, due to monotonicity, the FNN \hat{V}_ξ is designed to intrinsically satisfy the condition from (5).

Similarly, we incorporate the Lyapunov condition (4) into the training loss of (12) to impose the stability constraint

$$\min_{\theta} \mathbb{E}_{x(\cdot) \sim \rho} \left(\|f(x(t)) - \hat{f}_\theta(x(t : t - q + 1))\|^2 + [\hat{V}_\xi(\hat{f}_\theta(x_i(t : t - q + 1))) - \hat{V}_\xi(x)]^+ \right). \quad (17)$$

Here, the first term penalizes the difference in predicting the next state between \hat{f}_θ and f from (1); the second term penalizes the positive values of the discrete Lie derivative of \hat{V}_ξ for \hat{f}_θ , equivalent to the third term of (16). The first two terms of (16) are not included, as they are independent of \hat{f}_θ .

As done for (16), in practice we approximate the expected loss in (17) by using the sample average

$$\min_{\theta} \frac{1}{N} \sum_{i=1}^N \frac{1}{H - q - 1} \sum_{t=q-1}^{H-1} \left(\|f(x_i(t)) - \hat{f}_\theta(x_i(t : t - q + 1))\|^2 + [\hat{V}_\xi(\hat{f}_\theta(x_i(t : t - q + 1))) - \hat{V}_\xi(x_i(t))]^+ \right). \quad (18)$$

In training \hat{f}_θ via (18), we also impose the monotonicity constraints using the method from Sec. 3.2.

4 Case Studies

To evaluate effectiveness of our techniques, we consider two high-dimensional complex nonlinear dynamical systems that are monotone due to their physical properties.

Lotka-Volterra (LV) Model. We start with the LV model that describes the interaction of two cooperative groups (e.g., the males and the females of the same specie) occupying an environment

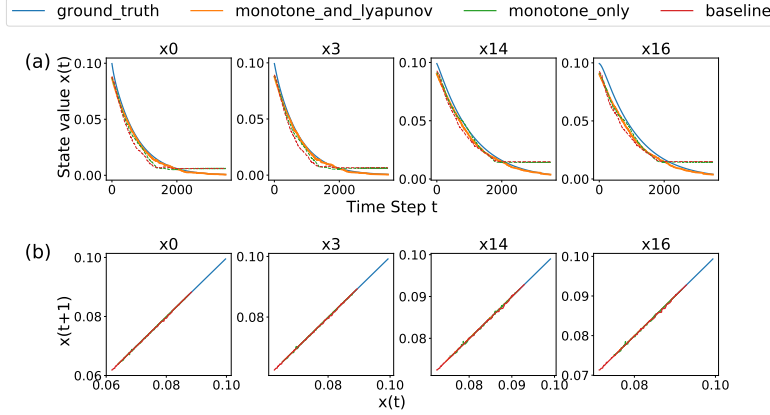


Figure 3: (a) Predicted trajectories of the LV model using 100-window up to 3500 time steps; (b) The $x(t+1)-x(t)$ relation of the predicted LV model trajectory up to 250 time steps.

of n discrete patches. For the group $k \in \{0, 1\}$, let $x_{ik}(t) \geq 0$ be the populations of the group k in the i^{th} patch at time $t \in \mathbb{N}$. The rate of migration from the j^{th} patch to the i^{th} patch is $a_{jik}x_{jk}(t)$ with $a_{jik} \geq 0$. At the patch i , the death rate is $b_{ik}x_{ik}(t)$, with $b_{ik} \geq 0$; and the reproduction rate is $c_{ik}x_{ik}(t)x_{i\bar{k}}(t)$, with $c_{ik} \geq 0$, where we make the convention that $\bar{k} = (k+1) \bmod 2$. Thus, for a discrete time step $\tau > 0$, the change of the populations of the two groups at the i^{th} patch is given by

$$x_{ik}(t+1) = x_{ik}(t) + \tau \left(c_{ik}x_{ik}(t)x_{i\bar{k}}(t) - b_{ik}x_{ik}(t) + \sum_{j \in [n] \setminus \{i\}} a_{jik}(x_{jk}(t) - x_{ik}(t)) \right). \quad (19)$$

The LV model is monotone on the positive orthant – if the population $x_{ik}(t)$ suddenly increases at time t for some i and k (e.g., adding new individuals from the outside), then the growth rate of all other populations will not decrease; thus, their populations only increase from the increment of $x_{ik}(t)$. To ensure that the time discretization in (19) faithfully captures this monotonicity property, the time step τ should satisfy $\tau < 1 / \max_{k \in \{1,2\}} \max_{i \in [n]} (b_{ik} + \sum_{j \in [n] \setminus \{i\}} a_{jik})$ for system (19) to be monotone.

Biochemical Control Circuit (BCC) Model. We also consider the BCC model describing the process of synthesizing protein from segments of mRNA E_0 in a cell, through a chain of enzymes E_1, \dots, E_n , where E_n is the end product. Let $x_0(t) \geq 0$ be the cellular concentration of mRNA, $x_i(t) \geq 0$ be the concentration of the enzyme i for $i \in [n]$ at time t . For each $i \in [n]$, the chemical reaction $\alpha_i E_{i-1} \rightarrow E_i$ is assumed to happen with unit rate, where $\alpha_i > 0$. In addition, the end product stimulate the creation of the mRNA by the rate $(x_n^p(t) + 1)/(x_n^p(t) + K)$ for some $K > 1$, and $p \in \mathbb{N}$. For a discrete time step $\tau > 0$, the change of the concentration of the enzyme i is given by

$$x_0(t+1) = x_0(t) + \tau \left(\frac{x_n^p(t) + 1}{x_n^p(t) + K} - \alpha_1 x_1(t) \right); \quad x_i(t+1) = x_i(t) + \tau (x_{i-1}(t) - \alpha_i x_i(t)). \quad (20)$$

The BCC model is monotone in the positive orthant, since if the increment of the concentration of the enzyme i will increase the concentration of the enzyme $i+1$ would increase too, and so on. To ensure that the time discretization in (20) does not violate this monotonicity property, the time step τ should satisfy $\tau < 1 / \max_{i \in [n]} \alpha_i$, for the system (20) to satisfy Lemma 1 – i.e., to be monotone.

Evaluation. We set $n = 10$ in (19) for the LV model and $n = 20$ in (20) for the BCC model, so the dimensions of the system states are 20 and 21, respectively. The training data are obtained from system trajectories initialized with a random set of initial states $x(0)$. More details on the selection of system constants, FNN architectures, and training hyper-parameters are provided in Appendix B.

We compare the performance when training the FNNs with (I) the proposed loss (18) that enforces both monotonicity and stability conditions, against (II) monotonicity loss (13) only (which does not ensure stability), and (III) mean-square loss only (i.e., neither monotonicity nor Lyapunov conditions are considered). We test the FNNs by iteratively predicting the system state T time steps (specifically $T = 1500, 2500, 3500$) after a given initial q -window of states that is not contained in the training data, and then compare with the ground truth. In all cases, the FNNs are trained for different windows sizes (specifically $q = 1, 100$), and the normalized ℓ^2 -norm errors, defined by the ratio of the ℓ^2 -norm of the prediction error to the ℓ^2 -norm of the ground truth, are summarized in Table 1. The

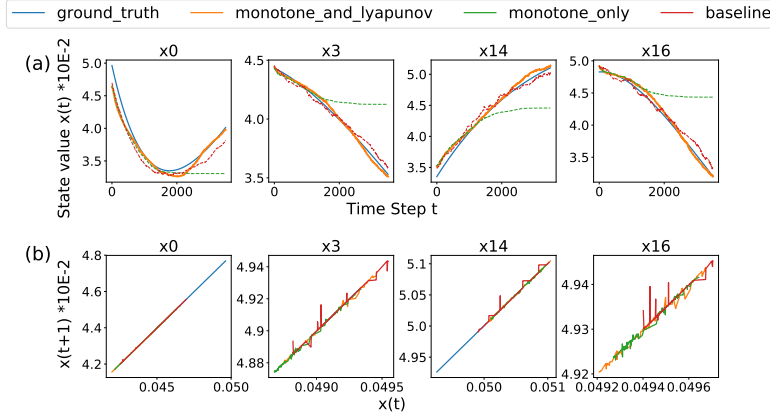


Figure 4: (a) Predicted trajectories of the BCC model using 100-window up to 3500 time steps; (b) The $x(t+1)-x(t)$ relation of the predicted BCC model trajectory up to 250 time steps.

Table 1: Normalized ℓ^2 -norm of Errors in Approximated Trajectories

	Monotone & Lyapunov		Monotone Only		Baseline	
LV Model						
Total Steps\Window	100	1	100	1	100	1
1500	0.1063	0.0514	0.1184	0.5114	0.1578	0.5700
2500	0.1070	0.0886	0.1262	0.9383	0.1628	1.0302
3500	0.1070	0.0966	0.1616	1.2983	0.1970	1.4143
BCC Model						
Total Steps\Window	100	1	100	1	100	1
1500	0.0359	0.2169	0.0397	0.2663	0.0376	1.6004
2500	0.0334	0.3878	0.0856	0.4514	0.0349	1.9314
3500	0.0330	0.5543	0.1746	0.6290	0.0377	2.2409

column headers “monotone and Lyapunov”, “monotone only” and “baseline” refer to training with the methods (I), (II) and (III) specified above.

The predicted trajectories for a subset of the states for the two case studies are shown in Figures 3(a) and 4(a), whereas the results for all states are provided in Figures 8 and 10 in Appendix D. Imposing either the monotonicity or the stability constraints reduces the prediction errors; and imposing both brings down the error even further. In addition, when the stability constraint is imposed (method (I)), the trained FNN becomes much more stable, which significantly reduces the prediction errors for long time horizons. Also, from Table 1, when condition (9) holds in the BCC model, using a longer window results in more accurate predictions of future states – the normalized ℓ^2 -norm of the prediction errors for the window size $q = 100$ is generally much smaller than that for the window size $q = 1$, except when method (I) is used for the LV model, since (9) does not hold for the LV model. In addition, the prediction errors ramp up much slower for $q = 100$ than $q = 1$ over long time horizons.

To validate monotonicity of the trained FNNs, we show in Figures 3(b) and 4(b) the $x(t+1)-x(t)$ relations for the first 250 steps for a selection of the dimensions of the states. The figures for all dimensions are given in Figures 9 and 11 in Appendix D. From the figures, the monotonicity condition is better satisfied holds when the monotonicity constraint is imposed in the training loss (in method (I) and (II)), despite the occasional violations due to the batch normalization. In addition, imposing the stability constraint (method (I)) generally does not worsen the violation of monotonicity.

5 Conclusion

We introduce a window-based method to learn the dynamics of unknown nonlinear monotone and stable dynamical systems. We employ feedforward neural network (FNNs) and capture these important physical properties of the system by imposing the corresponding monotonicity and stability constraints during training. On two high-dimensional complex nonlinear dynamical (biological and chemical) systems, we show that the combination of the monotonicity and stability constraints enforces both properties on the learned dynamics, while significantly reducing learning errors.

Broader Impact

Deep learning has found increasing applications for design and analysis of autonomous systems, such as driverless cars, unmanned aircraft, and (bio)medical devices and systems. Safety and performance guarantees for these autonomous systems critically depend on whether the employed deep learning components satisfy certain desirable properties and dynamical constraints. For example, as considered in this work, for biologically relevant analysis of population for Biochemical Control Circuits, it is important that the utilized learning-based models of the circuits preserve the properties of interest, such as stability and monotonicity.

While the problem of assuring autonomy has attracted significant attention in recent years, few previous studies have explored the aspect of deep learning in dynamical systems to provide assurance for learning-based design and analysis of autonomous systems. To fill the gap, this work proposes, to the best of our knowledge, the first method to impose the dynamical constraints, monotonicity and stability, to deep neural networks. Our techniques can be combined with previous studies on autonomous system design and analysis to provide assurance for such learning-based systems.

Acknowledgements

This work is sponsored in part by the ONR under agreement N00014-20-1-2745, AFOSR under award number FA9550-19-1-0169, as well as the NSF CNS-1652544 and CNS-1837499 awards.

References

- [1] Hal Smith. *Monotone Dynamical Systems: An Introduction to the Theory of Competitive and Cooperative Systems*, volume 41. 2008.
- [2] Samuel Coogan and Murat Arcak. Efficient finite abstraction of mixed monotone systems. In *Proceedings of the 18th International Conference on Hybrid Systems Computation and Control - HSCC '15*, pages 58–67, 2015.
- [3] Patrick De Leenheer, David Angeli, and Eduardo D. Sontag. Monotone Chemical Reaction Networks. *Journal of Mathematical Chemistry*, 41(3):295–314, 2007.
- [4] R. F. Costantino, J. M. Cushing, Brian Dennis, and Robert A. Desharnais. Experimentally induced transitions in the dynamic behaviour of insect populations. *Nature*, 375(6528):227–230, 1995.
- [5] Spencer M. Richards, Felix Berkenkamp, and Andreas Krause. The Lyapunov Neural Network: Adaptive Stability Certification for Safe Learning of Dynamical Systems. In *Proceedings of The 2nd Conference on Robot Learning*, pages 466–476, 2018.
- [6] Ya-Chien Chang, Nima Roohi, and Sicun Gao. Neural Lyapunov Control. In *Advances in Neural Information Processing Systems 32*, pages 3240–3249. 2019.
- [7] Hari Mukarjee and Steven Stern. Feasible Nonparametric Estimation of Multiargument Monotone Functions. *Journal of the American Statistical Association*, 89(425):77–80, 1994.
- [8] Arie Ben-David. Monotonicity Maintenance in Information-Theoretic Machine Learning Algorithms. *Machine Learning*, 19(1):29–43, 1995.
- [9] Klaus Neumann, Matthias Rolf, and Jochen J. Steil. Reliable integration of continuous constraints into extreme learning machines. *International Journal of Uncertainty, Fuzziness and Knowledge Based Systems*, 21(supp02):35–50, 2013.
- [10] Norman P. Archer and Shouhong Wang. Application of the Back Propagation Neural Network Algorithm with Monotonicity Constraints for Two-Group Classification Problems. *Decision Sciences*, 24(1):60–75, 1993.
- [11] Hennie Daniels and Marina Velikova. Monotone and Partially Monotone Neural Networks. *IEEE Transactions on Neural Networks*, 21(6):906–917, 2010.

- [12] Maya Gupta, Andrew Cotter, Jan Pfeifer, Konstantin Voevodski, Kevin Canini, Alexander Mangylov, Wojciech Moczydlowski, and Alexander van Esbroeck. Monotonic Calibrated Interpolated Look-Up Tables. page 47, 2016.
- [13] Joseph Sill. Monotonic Networks. In *Advances in Neural Information Processing Systems*, pages 661–667, 1998.
- [14] Seungil You, David Ding, Kevin Canini, Jan Pfeifer, and Maya Gupta. Deep Lattice Networks and Partial Monotonic Functions. In *Advances in Neural Information Processing Systems 30*, pages 2981–2989. 2017.
- [15] Pablo Márquez-Neila, Mathieu Salzmann, and Pascal Fua. Imposing hard constraints on deep networks: Promises and limitations. *arXiv preprint arXiv:1706.02025*, 2017.
- [16] Akhil Gupta, Naman Shukla, Lavanya Marla, Arinbjörn Kolbeinsson, and Kartik Yellepeddi. How to Incorporate Monotonicity in Deep Networks While Preserving Flexibility? *arXiv:1909.10662 [cs]*, 2019.
- [17] Joseph Sill and Yaser S. Abu-Mostafa. Monotonicity Hints. In *Advances in Neural Information Processing Systems 9*, pages 634–640. 1997.
- [18] Xin Chen, Erika Ábrahám, and Sriram Sankaranarayanan. Taylor Model Flowpipe Construction for Non-linear Hybrid Systems. In *2012 IEEE 33rd Real-Time Systems Symposium*, pages 183–192, 2012.
- [19] Antoine Wehenkel and Gilles Louppe. Unconstrained Monotonic Neural Networks. In *Advances in Neural Information Processing Systems*, pages 1543–1553, 2019.
- [20] Thao Dang, Oded Maler, and Romain Testylier. Accurate hybridization of nonlinear systems. In *Proceedings of the 13th ACM International Conference on Hybrid Systems: Computation and Control - HSCC '10*, page 11, 2010.
- [21] Shiyu Liang and R. Srikant. Why Deep Neural Networks for Function Approximation? In *The 5th International Conference on Learning Representations*, 2017.
- [22] J Zico Kolter and Gaurav Manek. Learning Stable Deep Dynamics Models. In *Advances in Neural Information Processing Systems*, pages 11126–11134, 2019.
- [23] Hassan K. Khalil. *Nonlinear Systems*. 3rd ed edition, 2002.
- [24] Hado Van Hasselt, Arthur Guez, and David Silver. Deep reinforcement learning with double q-learning. In *Thirtieth AAAI conference on artificial intelligence*, 2016.
- [25] Nitish Srivastava, Geoffrey Hinton, Alex Krizhevsky, Ilya Sutskever, and Ruslan Salakhutdinov. Dropout: a simple way to prevent neural networks from overfitting. *The journal of machine learning research*, 15(1):1929–1958, 2014.
- [26] Sergey Ioffe and Christian Szegedy. Batch normalization: Accelerating deep network training by reducing internal covariate shift. *arXiv preprint arXiv:1502.03167*, 2015.
- [27] James C Bezdek and Richard J Hathaway. Convergence of alternating optimization. *Neural, Parallel & Scientific Computations*, 11(4):351–368, 2003.
- [28] Anders Krogh and John A Hertz. A simple weight decay can improve generalization. In *Advances in neural information processing systems*, pages 950–957, 1992.

A Proofs

A.1 Proof of Lemma 2

Sketch of Proof. Let $x(t) = (x_1(t), \dots, x_n(t))$, $f(x) = (f_1(x), \dots, f_n(x))$ and $\hat{f}_\gamma(x) = (\hat{f}_1(x), \dots, \hat{f}_n(x))$. We first show that $\text{Var}_\gamma[x_i(t+T) - \hat{x}_i(t+T)] \gtrsim \left(\sum_{i=1}^T a^{2(i-1)}\right) \varepsilon^2/3$, where $x_i(t+T) = f_i(f^{(T-1)}(x(t)))$ and $\hat{x}_i(t+T) = \hat{f}_i(\hat{f}^{(T-1)}(x(t)))$.

From assumption (ii), it directly follows that

$$\mathbb{E}_\gamma[x_i(t+j) - \hat{x}_i(t+j)] = 0 \quad (21)$$

for all $j \in [1, T]$. Now, we prove by *induction* that

$$\text{Var}_\gamma[x_i(t+T) - \hat{x}_i(t+T)] \gtrsim \left(\sum_{i=1}^T a^{2(i-1)}\right) \varepsilon^2/3. \quad (22)$$

When $T = 1$, $\text{Var}_\gamma[x_i(t+1) - \hat{x}_i(t+1)] = \text{Var}_\gamma[\delta_i(x(t))] = \varepsilon^2/3$, which satisfies (22). Note that $\delta_i(x(\cdot))$ represents the i -th element in the one-step estimation error vector $\delta_\gamma(x(\cdot)) = f(x(\cdot)) - \hat{f}_\gamma(x(\cdot))$.

Let us assume that $\text{Var}_\gamma[x_i(t+T) - \hat{x}_i(t+T)] \gtrsim \left(\sum_{i=1}^T a^{2(i-1)}\right) \varepsilon^2/3$. We then need to show that $\text{Var}_\gamma[x_i(t+T+1) - \hat{x}_i(t+T+1)] \gtrsim \left(\sum_{i=1}^{T+1} a^{2(i-1)}\right) \varepsilon^2/3$.

First we can obtain

$$\text{Var}_\gamma[x_i(t+T+1) - \hat{x}_i(t+T+1)] = \text{Var}_\gamma[\hat{f}_i(\hat{x}(t+T))]. \quad (23)$$

Using Taylor series expansion, it can be obtained that

$$\begin{aligned} \text{Var}_\gamma[\hat{f}_i(\hat{x}(t+T))] &\approx \text{Var}_\gamma[\hat{f}_i(x(t+T))] + [\hat{f}'_i(x(t+T))]^2 \text{Var}_\gamma[x_i(t+T) - \hat{x}_i(t+T)] \\ &= \varepsilon^2/3 + [\hat{f}'_i(x(t+T))]^2 \text{Var}_\gamma[x_i(t+T) - \hat{x}_i(t+T)]. \end{aligned} \quad (24)$$

Also given that $\mathbb{E}[\hat{x}_i(t+T)] = x_i(t+T)$ from (21) and $\text{Var}_\gamma[x_i(t+T) - \hat{x}_i(t+T)] \gtrsim \left(\sum_{i=1}^T a^{2(i-1)}\right) \varepsilon^2/3$, it follows from (23) and (24) that

$$\text{Var}_\gamma[\hat{f}_i(\hat{x}(t+T))] \gtrsim \varepsilon^2/3 + [\hat{f}'_i(x(t+T))]^2 \left(\sum_{i=1}^T a^{2(i-1)}\right) \varepsilon^2/3 \quad (25)$$

$$\begin{aligned} &\geq \varepsilon^2/3 + a^2 \left(\sum_{i=1}^T a^{2(i-1)}\right) \varepsilon^2/3 \\ &= \left(\sum_{i=1}^{T+1} a^{2(i-1)}\right) \varepsilon^2/3, \end{aligned} \quad (26)$$

where the transition from (25) to (26) follows assumption (i) and (26) completes the proof of (22), and thus the lemma. \square

A.2 Proof of Theorem 1

Rationale of Theorem Assumptions. The intuition behind assumption (i) is that since all the NN weights are initialized at a positive random number that is very close to 0, and assume that the weights do not change drastically between any two consecutive gradient descent steps, which can be ensured by either Batch Normalization (BN) [26] or weight decay [28], then it is optimal for p_i 's converge to $1/q$ as in this case the Kullback–Leibler (KL) divergence between the initial weight distribution and $p_i \approx 1/q$ for all i is minimized. This assumption is numerically verified in Appendix C for the considered case study models from Section 4. Assumption (ii) is the same as assumption (i) of Lemma 2, capturing that f is a Lipschitz function and \hat{f}_{θ_i} 's in general capture the gradient properties of f . Note that if the constants a, b are not the same across all \hat{f}_{θ_i} 's, then we can perform a change of variable $a = \min_i a_i$ and $b = \max_i b_i$ to keep consistency. Assumption (iii) follows assumption (i), and in general captures that the window size q is sufficiently large compared to b . Finally, assumption (iv) follows the similar assumption from Lemma 2.

Let $x(t) = (x_1(t), \dots, x_n(t))$, $f(x) = (f_1(x), \dots, f_n(x))$ and $\hat{f}_{\theta_i} = (\hat{f}_{1,\theta_i}(x), \dots, \hat{f}_{n,\theta_i}(x))$ for all $i = 1, \dots, q$.

Sketch of Proof. We show that for all $j > 1, l = 1, \dots, n$

$$\text{Var}_{\theta}[x_l(t+j) - \hat{x}_l(t+j)] \lesssim \left(1 + \sum_{i=1}^q p_i^2 (b^2 + \varepsilon^2/3)\right) \frac{\varepsilon^2}{3q} \approx \left(1 + \frac{b^2 + \varepsilon^2/3}{q}\right) \frac{\varepsilon^2}{3q}.$$

To begin with, we first prove that

$$\text{Var}_{\theta}[x_l(t+j) - \hat{x}_l(t+j)] \lesssim \left(1 + \sum_{i=1}^q p_i^2 (b^2 + \varepsilon^2/3)\right) \frac{\varepsilon^2}{3q}. \quad (27)$$

For any $j = 1, \dots, q$, given a q -window of past states $x(t), x(t-1), \dots, x(t-q+1)$, we can obtain the following

$$\begin{aligned} & \text{Var}_{\theta}[x_l(t+j) - \hat{x}_l(t+j)] \\ &= \text{Var}_{\theta} \left[\sum_{i=1}^{j-1} p_i \left(f_l^{(i)}(x(t+j-i)) - \hat{f}_{l,\theta_i}(\hat{x}(t+j-i)) \right) \right. \\ & \quad \left. + \sum_{i=j}^q p_i \left(f_l^{(i)}(x(t+j-i)) - \hat{f}_{l,\theta_i}(x(t+j-i)) \right) \right] \\ &\leq \text{Var}_{\theta} \left[\sum_{i=1}^{j-1} p_i \left(f_l^{(i)}(x(t+j-i)) - \hat{f}_{l,\theta_i}(x(t+j-i)) - \hat{f}_{l,\theta_i}(\hat{x}(t+j-i)) \right) \right. \\ & \quad \left. + \sum_{i=j}^q p_i \delta_{l,\theta_i}(x(t+j-i)) \right] \quad (28) \\ &= \text{Var}_{\theta} \left[\sum_{i=1}^{j-1} p_i \left(\delta_{l,\theta_i}(x(t+j-i)) - \hat{f}_{l,\theta_i}(\hat{x}(t+j-i)) \right) + \sum_{i=j}^q p_i \delta_{l,\theta_i}(x(t+j-i)) \right] \\ &= \text{Var}_{\theta} \left[\sum_{i=1}^q p_i \delta_{l,\theta_i}(x(t+j-i)) - \sum_{i=1}^{j-1} p_i \hat{f}_{l,\theta_i}(\hat{x}(t+j-i)) \right] \\ &= \sum_{i=1}^q p_i^2 \text{Var}_{\theta} \left[\delta_{l,\theta_i}(x(t+j-i)) \right] + \sum_{i=1}^{j-1} p_i^2 \text{Var}_{\theta} \left[\hat{f}_{l,\theta_i}(\hat{x}(t+j-i)) \right], \quad (29) \end{aligned}$$

where $\delta_{l,\theta_i}(x(\cdot))$ represents the l -th element in the vector $\delta_{\theta_i}(x(t-i+1)) = \hat{f}_{\theta_i}(x(t-i+1)) - f^{(i)}(x(t-i+1))$ and $l = 1, \dots, n$. Note that the inequality in (28) holds because the term $\hat{f}_{l,\theta_i}(x(t+j-1))$ is introduced, which depends on θ_i and contains uncertainty.

Then we show by induction that for all $j = 1, \dots, q$,

$$\text{Var}_\theta [x_l(t+j) - \hat{x}_l(t+j)] \lesssim \left(1 + \sum_{i=1}^{j-1} p_i^2 (b^2 + \varepsilon^2/3)\right) \frac{\varepsilon^2}{3q}. \quad (30)$$

For $j = 1$,

$$\begin{aligned} & \text{Var}_\theta [x_l(t+1) - \hat{x}_l(t+1)] \\ & \leq \sum_{i=1}^q p_i^2 \text{Var}_\theta [\delta_{l,\theta_i}(x(t+j-i))] + \sum_{i=1}^{j-1} p_i^2 \text{Var}_\theta [\hat{f}_{l,\theta_i}(\hat{x}(t+j-1))] \\ & = \sum_{i=1}^q p_i^2 \varepsilon^2/3 \approx \frac{\varepsilon^2}{3q}, \end{aligned}$$

where the last transition follows condition (i) and satisfies (30).

Assuming for $j = k-1 \leq q-1$,

$$\text{Var}_\theta [x_l(t+k-1) - \hat{x}_l(t+k-1)] \lesssim \left(1 + \sum_{i=1}^{k-2} p_i^2 (b^2 + \varepsilon^2/3)\right) \frac{\varepsilon^2}{3q} \quad (31)$$

holds, we prove the same holds for $j = k$ as follows

$$\text{Var}_\theta [x_l(t+k) - \hat{x}_l(t+k)] \quad (32)$$

$$\leq \sum_{i=1}^q p_i^2 \text{Var}_\theta [\delta_{l,\theta_i}(x(t+k-i))] + \sum_{i=1}^{k-1} p_i^2 \text{Var}_\theta [\hat{f}_{l,\theta_i}(\hat{x}(t+k-1))] \quad (33)$$

$$\approx \sum_{i=1}^q p_i^2 \varepsilon^2/3 + \sum_{i=1}^{k-1} p_i^2 \left(\varepsilon^2/3 + [\hat{f}'_{l,\theta_i}(x(t+k-1))]^2 \right) \left(1 + \sum_{m=1}^{k-2} p_m^2 (b^2 + \varepsilon^2/3) \right) \frac{\varepsilon^2}{3q} \quad (34)$$

$$\leq \frac{\varepsilon^2}{3q} + \sum_{i=1}^{k-1} \left(p_i^2 (b^2 + \varepsilon^2/3) + p_i^2 (b^2 + \varepsilon^2/3) \sum_{m=1}^{k-2} p_m^2 (b^2 + \varepsilon^2/3) \right) \frac{\varepsilon^2}{3q} \quad (35)$$

$$\approx \frac{\varepsilon^2}{3q} + \sum_{i=1}^{k-1} p_i^2 (b^2 + \varepsilon^2/3) \frac{\varepsilon^2}{3q}, \quad (36)$$

which completes the proof for $j = 1, \dots, q$.

The transition between (32) and (33) follows directly from (28). The transition between (33) and (34) is obtained from the following fact. It is easy to see that $\mathbb{E}[x_l(t+i) - \hat{x}_l(t+i)] = 0$ for all $i = 1, \dots, T$ given condition (iv). Then using Taylor series expansion and take variance for both sides of the equation, it can be obtained that

$$\begin{aligned} & \text{Var}_\theta [\hat{f}_{l,\theta_i}(\hat{x}(t+j))] \\ & \approx \text{Var}_\theta [\hat{f}_{l,\theta_i}(x(t+j))] + [\hat{f}'_{l,\theta_i}(x(t+j))]^2 \text{Var}_\theta [x_l(t+j) - \hat{x}_l(t+j)] \\ & = \varepsilon^2/3 + [\hat{f}'_{l,\theta_i}(x(t+j))]^2 \text{Var}_\theta [x_l(t+j) - \hat{x}_l(t+j)]. \end{aligned} \quad (37)$$

The transition between (34) and (35) follows condition (i) and (ii), and the drop of term $p_i^2 (b^2 + \varepsilon^2/3) \sum_{m=1}^{k-2} p_m^2 (b^2 + \varepsilon^2/3)$ between (35) and (36) follows the condition (iii).

We now show that (27) holds for $j > q$. First, we have the following for all $j > q$ that

$$\begin{aligned} & \text{Var}_\theta [x_l(t+j) - \hat{x}_l(t+j)] \\ &= \text{Var}_\theta \left[\sum_{i=1}^q p_i \left(f_l^{(i)}(x(t+j-i)) - \hat{f}_{l,\theta_i}(\hat{x}(t+j-1)) \right) \right] \\ &\leq \text{Var}_\theta \left[\sum_{i=1}^q p_i (f_l^{(i)}(x(t+j-i)) - \hat{f}_{l,\theta_i}(x(t+j-i)) - \hat{f}_{l,\theta_i}(\hat{x}(t+j-1))) \right] \end{aligned} \quad (38)$$

$$\begin{aligned} &= \text{Var}_\theta \left[\sum_{i=1}^q p_i \delta_{l,\theta_i}(x(t+j-i)) + \sum_{i=1}^q p_i \hat{f}_{l,\theta_i}(\hat{x}(t+j-1)) \right] \\ &= \sum_{i=1}^q p_i^2 \text{Var}_\theta [\delta_{l,\theta_i}(x(t+j-i))] + \sum_{i=1}^q p_i^2 \text{Var}_\theta [\hat{f}_{l,\theta_i}(\hat{x}(t+j-1))] \end{aligned} \quad (39)$$

$$\approx \frac{\varepsilon^2}{3q} + \sum_{i=1}^q p_i^2 \text{Var}_\theta [\hat{f}_{l,\theta_i}(\hat{x}(t+j-1))], \quad (40)$$

where the inequality holds in (38) because the term $\hat{f}_{l,\theta_i}(x(t+j-1))$ is introduced, which depend on θ_i and contains uncertainty. The transition between (39) and (40) due to condition (i).

We now show by induction that for all $j > q$,

$$\text{Var}_\theta [x_l(t+j) - \hat{x}_l(t+j)] \lesssim \left(1 + \sum_{i=1}^q p_i^2 (b^2 + \varepsilon^2/3)\right) \frac{\varepsilon^2}{3q}. \quad (41)$$

First, for $j = q + 1$,

$$\text{Var}_\theta [x_l(t+q+1) - \hat{x}_l(t+q+1)] \quad (42)$$

$$\approx \frac{\varepsilon^2}{3q} + \sum_{i=1}^q p_i^2 \text{Var}_\theta [\hat{f}_{l,\theta_i}(\hat{x}(t+q))] \quad (43)$$

$$\approx \frac{\varepsilon^2}{3q} + \sum_{i=1}^q p_i^2 \left(\varepsilon^2/3 + [\hat{f}'_{l,\theta_i}(x(t+q))]^2 \right) \left(1 + \sum_{m=1}^{q-1} p_m^2 (b^2 + \varepsilon^2/3) \right) \frac{\varepsilon^2}{3q} \quad (44)$$

$$\leq \frac{\varepsilon^2}{3q} + \sum_{i=1}^q p_i^2 (b^2 + \varepsilon^2/3) \left(1 + \sum_{m=1}^{q-1} p_m^2 (b^2 + \varepsilon^2/3) \right) \frac{\varepsilon^2}{3q} \quad (45)$$

$$= \frac{\varepsilon^2}{3q} + \sum_{i=1}^q \left(p_i^2 (b^2 + \varepsilon^2/3) + p_i^2 (b^2 + \varepsilon^2/3) \sum_{m=1}^{q-1} p_m^2 (b^2 + \varepsilon^2/3) \right) \frac{\varepsilon^2}{3q} \quad (46)$$

$$\approx \left(1 + \sum_{i=1}^q p_i^2 (b^2 + \varepsilon^2/3) \right) \frac{\varepsilon^2}{3q}, \quad (47)$$

which satisfies (41). The transition between (42) and (43) follows directly from (40). The transition between (43) and (44) follows (37). The inequality between (44) and (45) holds because of assumption (ii). The term $p_i^2 (b^2 + \varepsilon^2/3) \sum_{m=1}^{q-1} p_m^2 (b^2 + \varepsilon^2/3)$ from (46) is dropped in (47) due to the condition (iii).

Assuming that for $j = k - 1 > q$,

$$\text{Var}_\theta [x_l(t+k-1) - \hat{x}_l(t+k-1)] \lesssim \left(1 + \sum_{i=1}^q p_i^2 (b^2 + \varepsilon^2/3) \right) \frac{\varepsilon^2}{3q}$$

holds, and we prove the same holds for $j = k$ as follows

$$\text{Var}_\theta [x_l(t+k) - \hat{x}_l(t+k)] \quad (48)$$

$$\approx \frac{\varepsilon^2}{3q} + \sum_{i=1}^q p_i^2 \text{Var}_\theta [\hat{f}_{l,\theta_i}(\hat{x}(t+k-1))] \quad (49)$$

$$\leq \frac{\varepsilon^2}{3q} + \sum_{i=1}^q p_i^2 \left(\varepsilon^2/3 + [\hat{f}'_{l,\theta_i}(x(t+k-1))]^2 \right) \left(1 + \sum_{m=1}^q p_m^2 (b^2 + \varepsilon^2/3) \right) \frac{\varepsilon^2}{3q} \quad (50)$$

$$\leq \frac{\varepsilon^2}{3q} + \sum_{i=1}^q p_i^2 (b^2 + \varepsilon^2/3) \left(1 + \sum_{m=1}^q p_m^2 (b^2 + \varepsilon^2/3) \right) \frac{\varepsilon^2}{3q} \quad (51)$$

$$= \frac{\varepsilon^2}{3q} + \sum_{i=1}^q (p_i^2 (b^2 + \varepsilon^2/3) + p_i^2 b^2 \sum_{m=1}^q p_m^2 (b^2 + \varepsilon^2/3)) \frac{\varepsilon^2}{3q} \quad (52)$$

$$\approx \frac{\varepsilon^2}{3q} + \sum_{i=1}^q p_i^2 (b^2 + \varepsilon^2/3) \frac{\varepsilon^2}{3q}, \quad (53)$$

which completes the proof of (27) for $j > q$. Specifically, the transition between (48) and (49) follows from (40). Then the inequality between (49) and (50) holds due to (37), and the inequality between (50) and (51) holds because of assumption (ii). And the term $p_i^2 (b^2 + \varepsilon^2/3) \sum_{m=1}^{q-1} p_m^2 (b^2 + \varepsilon^2/3)$ is dropped while transferring to (53) from (52) because of condition (iii).

To summarize, for any $j \geq 1$, we have

$$\text{Var}_\theta [x_l(t+j) - \hat{x}_l(t+j)] \lesssim \left(1 + \sum_{i=1}^q p_i^2 (b^2 + \varepsilon^2/3) \right) \frac{\varepsilon^2}{3q} \approx \left(1 + \frac{b^2 + \varepsilon^2/3}{q} \right) \frac{\varepsilon^2}{3q}, \quad (54)$$

which completes the proof. \square

A.3 Proof of Claim 1

We prove that the FNN \hat{f}_θ from Section 3.2 is convex if it only uses the max-ReLU neurons from (14). First, the activation function of max-ReLU neurons from (14) is convex and monotonically non-decreasing, when $\theta_1, \dots, \theta_n \geq 0$.

Claim 2: The composition of such convex and monotonically non-decreasing functions is still convex and monotonically non-decreasing.

This is because, for convex and monotonically non-decreasing functions $\psi, \varphi_1, \dots, \varphi_m$ of proper dimensions, it holds that for any x_1 and x_2

$$\begin{aligned} & \psi\left(\varphi_1\left(\frac{x_1 + x_2}{2}\right), \dots, \varphi_m\left(\frac{x_1 + x_2}{2}\right)\right) \\ & \leq \psi\left(\frac{\varphi_1(x_1) + \varphi_1(x_2)}{2}, \dots, \frac{\varphi_m(x_1) + \varphi_m(x_2)}{2}\right) \\ & \leq \frac{\psi(\varphi_1(x_1), \dots, \varphi_m(x_1)) + \psi(\varphi_1(x_2), \dots, \varphi_m(x_2))}{2}, \end{aligned}$$

where the first inequality holds due to the monotonicity of ψ and the convexity of $\varphi_1, \dots, \varphi_m$, and the second inequality holds due to the convexity of ψ . Thus, the composition $\psi(\varphi_1(x), \dots, \varphi_m(x))$ is convex for x . The function $\psi(\varphi_1(x), \dots, \varphi_m(x))$ is also monotonically non-decreasing, due to the monotonicity of $\psi, \varphi_1, \dots, \varphi_m$.

Now, for an FNN \hat{f}_θ composed of only max-ReLU neurons, we can inductively apply **Claim 2** over the layers of the FNN (as in the proof in Appendix A.4) to show that \hat{f}_θ is convex (as well as monotonically non-decreasing). \square

A.4 Proof of Theorem 2

From (14), since the weights satisfy $\theta_1, \dots, \theta_d \geq 0$, it follows that the activation function φ of each neuron is monotonically non-decreasing. For an FNN \hat{f}_θ that is composed of such neurons, we can inductively prove the output of the first layer is monotonically non-decreasing with the inputs; the output of the second layer is monotonically non-decreasing for the inputs; and so on. Hence, \hat{f}_θ is monotone. \square

B Experimental and Training Details

In this section, we provide details regarding the parameter selection of the case study models and neural network training.

B.1 Model Parameter Selection

For each model, the training data batch is filled with the state visitation sequences generated by executing 20 trajectories following the corresponding system dynamics for 5000 time steps $\{x^{(1)}(0 : 5000), \dots, x^{(20)}(0 : 5000)\}$, where each one evolves from a unique initial state. Then, the network \hat{f} is trained to learn the one step mapping $x^{(\cdot)}(t : t - q + 1) \rightarrow x^{(\cdot)}(t + 1)$, where $x(t : t - q + 1)$ denotes the q -window of previous states $x(t), \dots, x(t - q + 1)$

Specifically, for the LV Model, a_{jik}, b_{ik} and c_{ik} for all $i \in [0, 9], j \in [0, 9]$ are selected to be random numbers uniformly sampled from $[0, 5]$ and $\tau = 0.0005$. For the BCC Model, $n = 20, k = 8, p = 10$ and all elements in α is sampled uniformly from $[0, 10]$.

B.2 Neural Network Architectures and Learning Hyper-parameters

For the models in our case studies (Section 4), both \hat{f}_θ and \hat{V}_ξ are designed to have two hidden layers where each one contains 2000 nodes. We designed the activation function of the output layer of the network \hat{V}_ξ as

$$o = \max_n \{W_{n \times h}^T o_h + z_n\},$$

where n is the system dimension, o_h is the output from the last hidden layer with h neurons, $W_{n \times h}$ represents the weight of output layer, z_n is the bias term and the final output o is obtained by selecting the maximum value over n dimensions, as shown in Figure 5 for a general system model (i.e., with potentially more than two layers used in the case study models). Then the network intrinsically satisfies the form of Lyapunov functions in monotone systems specified in (5).

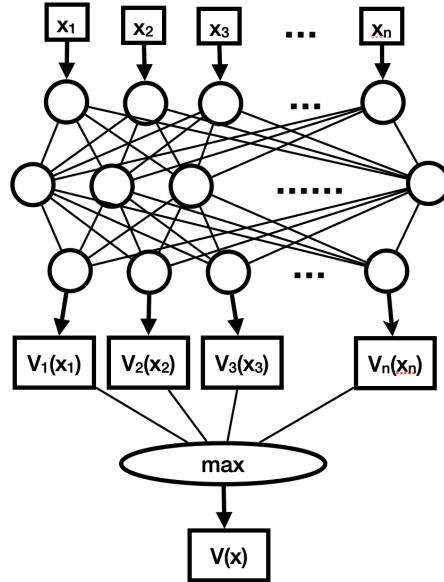


Figure 5: General Architecture of \hat{V}_ξ .

The learning rate for \hat{f}_θ and \hat{V}_ξ is set to be 10^{-4} , and 10^{-5} , respectively. Exponential decay of 0.98 in each 250 steps are applied to both learning rates. Batch training is also performed to further reduce the variance that might occur during the back-propagation process, where in each step 500 samples are randomly acquired from the training dataset. Furthermore, during training a 0.01 weight decay is applied to both networks to prevent the parameters from changing drastically between any two consecutive gradient descent steps. Two networks are trained alternately in each step with Adam

optimizer for a total of 400,000 epochs. The machine used to train the networks is configured with 3 Nvidia Quadro RTX 6000 graphic cards, 2 Intel Xeon Silver 4208 2.1GHz CPUs and 192 GB RAM.

C Numerical Verification of Additional Condition (i) in Theorem 1

In this section, we verify that for both case studies described in Section 4, the assumption (i) of Theorem 1 is satisfied. When 100-window is used, most weights of the output layer of \hat{f}_θ are distributed within $[-0.01, 0.01]$; specifically all are within $[0, 0.01]$ for the BCC model, where as for the LV model all are within $[-0.01, 0.015]$. This can be observed from Figure 6 and Figure 7, which visualizes the histogram of output layer weights for the NN capturing dynamics of LV and BCC model respectively.

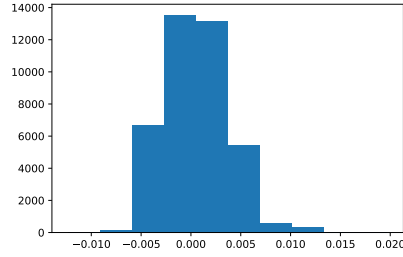


Figure 6: Histogram of output layer weights in the LV model.

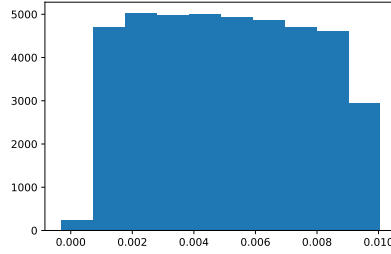


Figure 7: Histogram of output layer weights in the BCC model.

D Supplemental Results and Figures

Table 2: Normalized ℓ^2 -norm of Errors in Approximated Trajectories for each Dimension of LV model over horizon $T = 3500$

Dimension \ Window	Monotone & Lyapunov		Monotone Only		Baseline	
	100	1	100	1	100	1
x_0	0.1456	0.1328	0.2684	3.0545	0.3531	3.2832
x_1	0.2296	0.0802	0.3482	3.0141	0.4364	3.2381
x_2	0.2335	0.09	0.3591	3.0277	0.4465	3.2531
x_3	0.1345	0.1349	0.2592	3.0968	0.3552	3.3265
x_4	0.262	0.0798	0.3123	3.0209	0.3954	3.2477
x_5	0.213	0.0928	0.3134	3.0144	0.3993	3.2389
x_6	0.2169	0.0789	0.4021	3.0545	0.4926	3.2808
x_7	0.2291	0.0823	0.3569	3.0429	0.4517	3.2684
x_8	0.3488	0.1286	0.4139	3.0199	0.5105	3.2412
x_9	0.3541	0.111	0.4062	3.0528	0.5006	3.2763
x_{10}	0.1392	0.2819	0.296	2.3677	0.3374	2.6381
x_{11}	0.322	0.3638	0.3805	2.3332	0.486	2.5908
x_{12}	0.129	0.2853	0.2785	2.3902	0.3221	2.6625
x_{13}	0.3737	0.4041	0.3852	2.3197	0.488	2.5749
x_{14}	0.2051	0.3091	0.3114	2.3587	0.4004	2.6254
x_{15}	0.0834	0.2892	0.3307	2.4033	0.3144	2.6809
x_{16}	0.3071	0.3785	0.3885	2.3177	0.4987	2.5752
x_{17}	0.2922	0.3408	0.3448	2.3311	0.4368	2.5904
x_{18}	0.1169	0.3388	0.3762	2.4665	0.3319	2.752
x_{19}	0.2251	0.3053	0.2957	2.3604	0.3609	2.629

Table 3: Normalized ℓ^2 -norm of Errors in Approximated Trajectories for each Dimension of BCC model over horizon $T = 3500$

Dimension \ Window	Monotone & Lyapunov		Monotone Only		Baseline	
	100	1	100	1	100	1
x_0	0.0664	0.4348	0.1568	0.6076	0.084	6.8689
x_1	0.0774	1.3755	0.3475	1.6032	0.0755	4.1152
x_2	0.0495	0.9741	0.3871	1.0639	0.0658	3.7122
x_3	0.0137	0.2872	0.1507	0.2927	0.0217	4.6587
x_4	0.1013	1.3998	0.3165	1.6685	0.0996	4.093
x_5	0.0974	1.4825	0.3934	1.7086	0.1025	3.9049
x_6	0.0899	1.5043	0.3853	1.7461	0.0913	3.9428
x_7	0.0625	1.1657	0.4224	1.2771	0.0787	3.659
x_8	0.0832	1.3892	0.3966	1.59	0.088	3.8447
x_9	0.0497	1.0729	0.4086	1.1771	0.0657	3.6744
x_{10}	0.0916	1.3968	0.3819	1.6066	0.0985	3.8821
x_{11}	0.0588	1.0652	0.4026	1.1613	0.0766	3.6557
x_{12}	0.0314	0.7192	0.312	0.7706	0.0451	3.9074
x_{13}	0.0476	0.8613	0.3289	0.9402	0.0612	3.8579
x_{14}	0.0218	0.2861	0.0905	0.3144	0.0228	6.6869
x_{15}	0.0675	1.1237	0.3193	1.278	0.0737	4.0916
x_{16}	0.0115	0.2255	0.1262	0.2203	0.0198	4.9192
x_{17}	0.0235	0.5387	0.2232	0.5854	0.0337	4.4051
x_{18}	0.0515	1.0439	0.3584	1.1663	0.0634	3.874
x_{19}	0.0284	0.6649	0.2938	0.7098	0.0436	4.0075
x_{20}	0.0312	0.6013	0.2525	0.6394	0.0437	4.1388

Table 4: Normalized ℓ^2 -norm of Errors in Approximated Trajectories for each Dimension of LV model over horizon $T = 2500$

Dimension \ Window	Monotone & Lyapunov		Monotone Only		Baseline	
	100	1	100	1	100	1
x_0	0.1454	0.1291	0.2295	2.2826	0.322	2.4691
x_1	0.2294	0.0745	0.3251	2.2445	0.4139	2.4265
x_2	0.2334	0.0853	0.3332	2.2566	0.4261	2.4399
x_3	0.134	0.1315	0.2145	2.3142	0.3167	2.5014
x_4	0.2617	0.0743	0.2826	2.2459	0.3689	2.4297
x_5	0.2129	0.0875	0.2908	2.2456	0.3752	2.4281
x_6	0.2167	0.0727	0.3806	2.2703	0.4742	2.4537
x_7	0.2289	0.0767	0.3316	2.2626	0.4253	2.4455
x_8	0.3482	0.1255	0.3934	2.234	0.4939	2.412
x_9	0.3536	0.107	0.3869	2.2624	0.4819	2.4427
x_{10}	0.1389	0.2476	0.1223	1.6266	0.1722	1.8369
x_{11}	0.3204	0.3296	0.2963	1.5897	0.4172	1.7832
x_{12}	0.1287	0.2526	0.1128	1.6462	0.1709	1.86
x_{13}	0.3723	0.3702	0.2867	1.5746	0.4086	1.7616
x_{14}	0.2042	0.2722	0.1779	1.6124	0.292	1.8166
x_{15}	0.0826	0.2606	0.1691	1.6633	0.108	1.8826
x_{16}	0.3053	0.3431	0.2957	1.5746	0.4211	1.7656
x_{17}	0.2909	0.3054	0.232	1.5888	0.3438	1.7844
x_{18}	0.1156	0.3182	0.2302	1.7244	0.12	1.9538
x_{19}	0.2247	0.2678	0.1481	1.6159	0.2348	1.8226

Table 5: Normalized ℓ^2 -norm of Errors in Approximated Trajectories for each Dimension of BCC model over horizon $T = 2500$

Dimension \ Window	Monotone & Lyapunov		Monotone Only		Baseline	
	100	1	100	1	100	1
x_0	0.0659	0.3897	0.0646	0.531	0.0667	5.8096
x_1	0.0767	0.9538	0.1804	1.14	0.0717	3.2538
x_2	0.0448	0.6029	0.1619	0.6762	0.0539	2.9196
x_3	0.0096	0.1725	0.0543	0.1767	0.0126	3.8664
x_4	0.1009	0.9882	0.1776	1.2071	0.0976	3.2437
x_5	0.0962	1.0157	0.2038	1.2	0.0987	3.0464
x_6	0.0891	1.0407	0.2007	1.2382	0.0868	3.0845
x_7	0.0588	0.741	0.1851	0.8319	0.0697	2.846
x_8	0.0818	0.9397	0.1954	1.1038	0.0821	3.0019
x_9	0.0465	0.676	0.1754	0.7615	0.0509	2.8756
x_{10}	0.0904	0.9518	0.1946	1.1228	0.0939	3.0369
x_{11}	0.0536	0.6669	0.1711	0.7454	0.0679	2.8564
x_{12}	0.0272	0.4375	0.1247	0.4797	0.0286	3.1391
x_{13}	0.0432	0.5394	0.1385	0.6038	0.0528	3.0737
x_{14}	0.0189	0.1932	0.0403	0.2148	0.0209	5.7067
x_{15}	0.0664	0.7596	0.156	0.8854	0.069	3.2575
x_{16}	0.0104	0.141	0.0467	0.1373	0.0091	4.1026
x_{17}	0.0223	0.3404	0.093	0.3784	0.0205	3.6096
x_{18}	0.0495	0.6777	0.1603	0.7779	0.0523	3.0665
x_{19}	0.0257	0.4032	0.1169	0.4399	0.0263	3.2352
x_{20}	0.0267	0.3675	0.1001	0.3984	0.0351	3.3614

Table 6: Normalized ℓ^2 -norm of Errors in Approximated Trajectories for each Dimension of LV model over horizon $T = 1500$

Dimension \ Window	Monotone & Lyapunov		Monotone Only		Baseline	
	100	1	100	1	100	1
x_0	0.1434	0.119	0.2122	1.302	0.3142	1.4353
x_1	0.2259	0.0549	0.3114	1.2677	0.4062	1.3962
x_2	0.2293	0.0688	0.3179	1.2779	0.4174	1.4078
x_3	0.1322	0.1215	0.1979	1.3197	0.3082	1.4536
x_4	0.2596	0.0529	0.2658	1.2625	0.3614	1.3911
x_5	0.2094	0.0728	0.2718	1.2699	0.3673	1.399
x_6	0.2122	0.0513	0.3656	1.2752	0.4666	1.4038
x_7	0.2261	0.0575	0.3174	1.272	0.4179	1.4001
x_8	0.3436	0.1109	0.3787	1.2382	0.4863	1.3596
x_9	0.3491	0.0917	0.3719	1.2603	0.4742	1.3844
x_{10}	0.1347	0.054	0.0909	0.7941	0.1478	0.9168
x_{11}	0.3088	0.1735	0.2744	0.7861	0.4031	0.8769
x_{12}	0.1246	0.0914	0.0766	0.8031	0.1487	0.9339
x_{13}	0.361	0.2224	0.267	0.7875	0.3953	0.8606
x_{14}	0.1962	0.0704	0.1518	0.7882	0.2776	0.8968
x_{15}	0.0818	0.1334	0.1473	0.8198	0.0633	0.9581
x_{16}	0.2936	0.1879	0.2741	0.7819	0.407	0.8639
x_{17}	0.2806	0.1351	0.2115	0.783	0.3302	0.8772
x_{18}	0.1127	0.2424	0.2101	0.8671	0.0648	1.0224
x_{19}	0.2186	0.0661	0.1208	0.7889	0.2178	0.902

Table 7: Normalized ℓ^2 -norm of Errors in Approximated Trajectories for each Dimension of BCC model over horizon $T = 1500$

Dimension \ Window	Monotone & Lyapunov		Monotone Only		Baseline	
	100	1	100	1	100	1
x_0	0.06	0.2538	0.0588	0.349	0.0631	4.4175
x_1	0.0753	0.4895	0.08	0.6235	0.0706	2.2556
x_2	0.0438	0.2745	0.0519	0.3257	0.0522	2.0671
x_3	0.0073	0.1076	0.0079	0.1098	0.0109	2.9466
x_4	0.1002	0.5221	0.1042	0.6775	0.0968	2.2437
x_5	0.0955	0.5128	0.1063	0.644	0.0975	2.0669
x_6	0.0876	0.5344	0.0986	0.6759	0.0856	2.0983
x_7	0.0577	0.3441	0.0683	0.4083	0.0677	1.9706
x_8	0.0805	0.4702	0.0894	0.5872	0.0809	2.0524
x_9	0.0436	0.3139	0.0522	0.3748	0.0486	2.016
x_{10}	0.0895	0.4798	0.1004	0.601	0.0928	2.0765
x_{11}	0.0529	0.3055	0.0636	0.3604	0.0657	1.9981
x_{12}	0.0246	0.2063	0.0267	0.2355	0.0263	2.2966
x_{13}	0.0426	0.2537	0.0497	0.2982	0.0512	2.212
x_{14}	0.0182	0.1186	0.0199	0.1301	0.0193	4.4722
x_{15}	0.0655	0.3806	0.0687	0.4698	0.0679	2.3034
x_{16}	0.0074	0.1	0.0083	0.0985	0.0068	3.143
x_{17}	0.0187	0.174	0.0195	0.1995	0.0172	2.6971
x_{18}	0.0475	0.327	0.0543	0.3983	0.0503	2.1718
x_{19}	0.0224	0.1916	0.0234	0.2167	0.023	2.3819
x_{20}	0.0263	0.1781	0.0295	0.1984	0.0338	2.4895

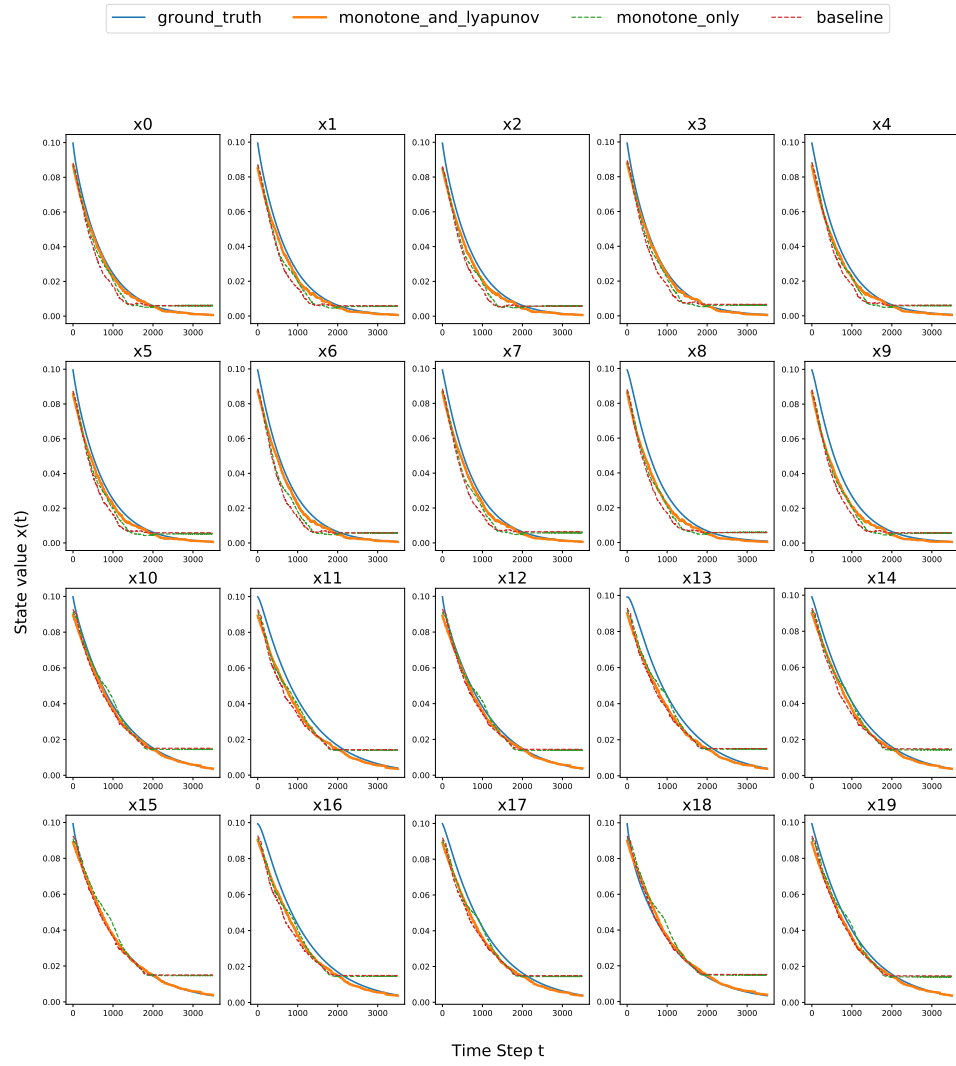


Figure 8: Predicted trajectories of the LV model using 100-window up to 3500 time steps

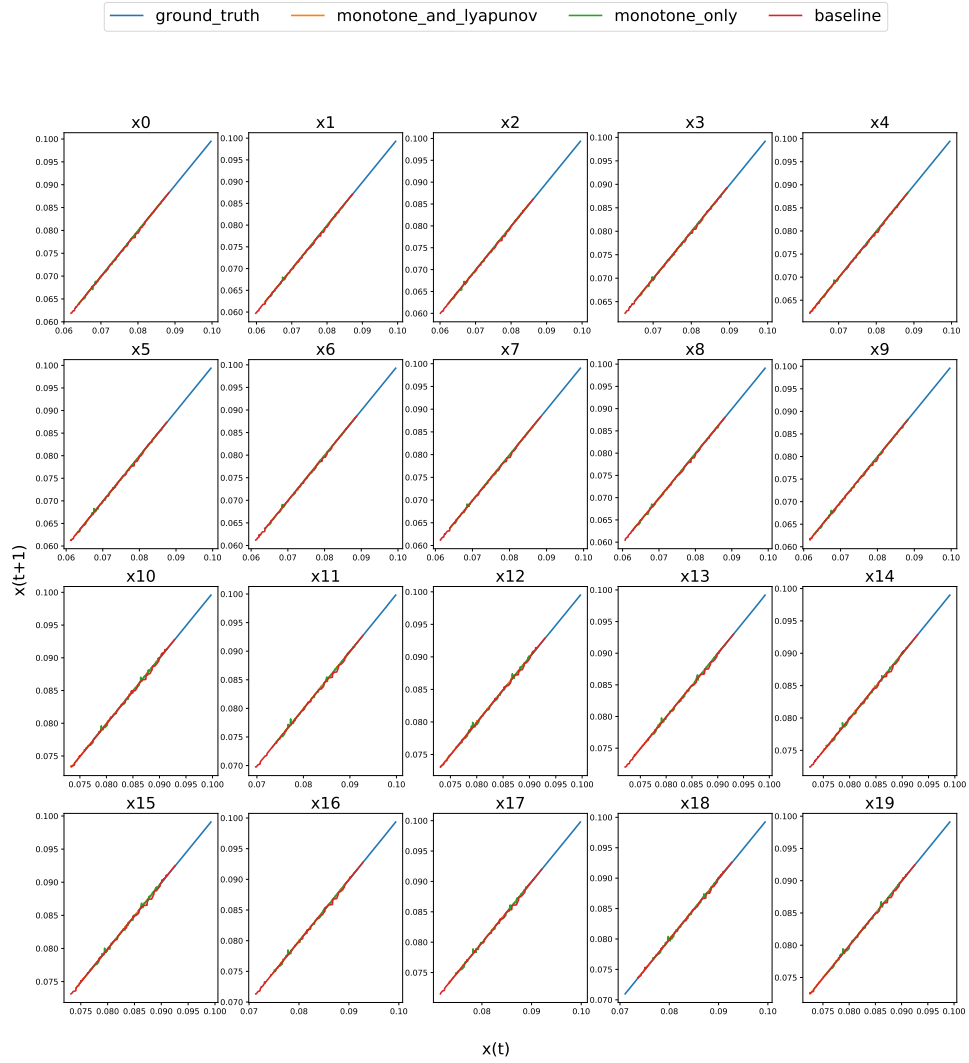


Figure 9: The $x(t + 1)-x(t)$ relation of the predicted LV model trajectory up to 250 time steps using 100-window.

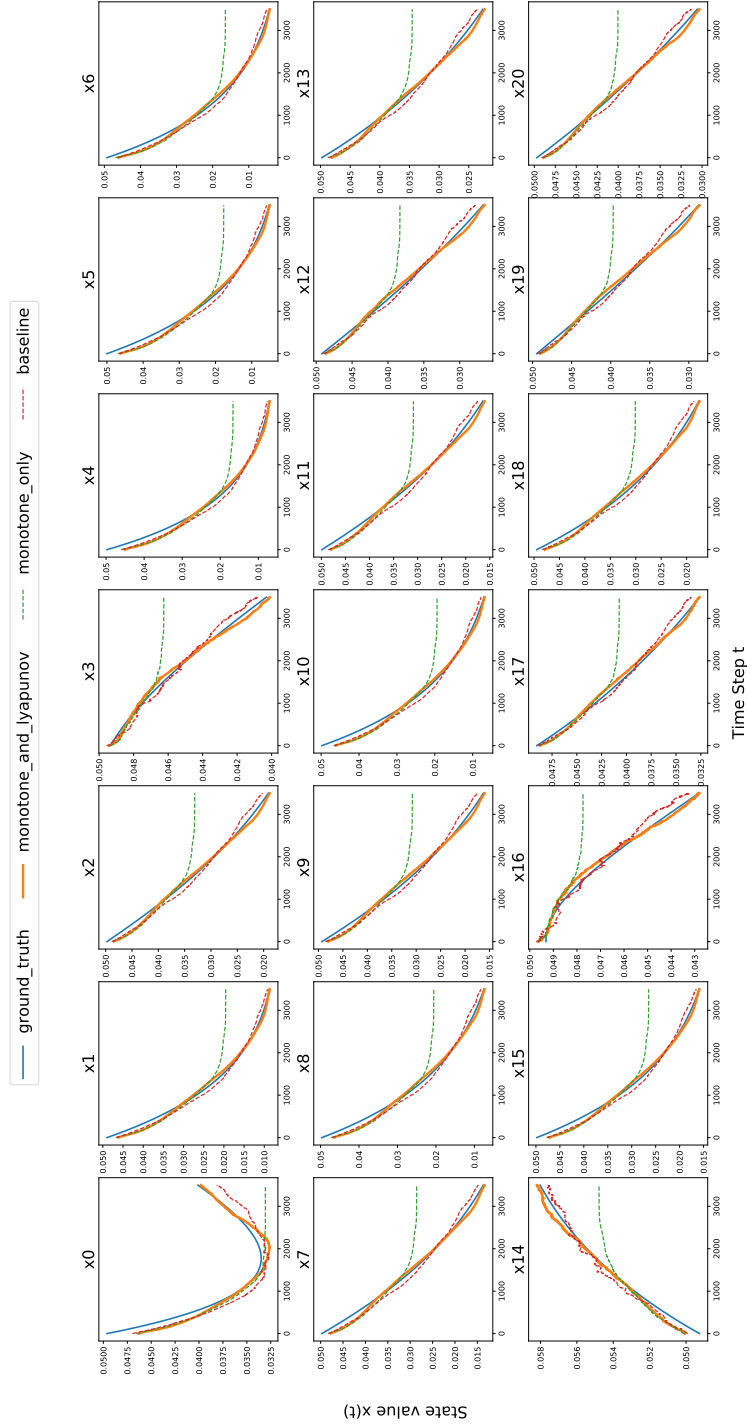


Figure 10: Predicted trajectories of the BCC model using 100-window up to 3500 time steps

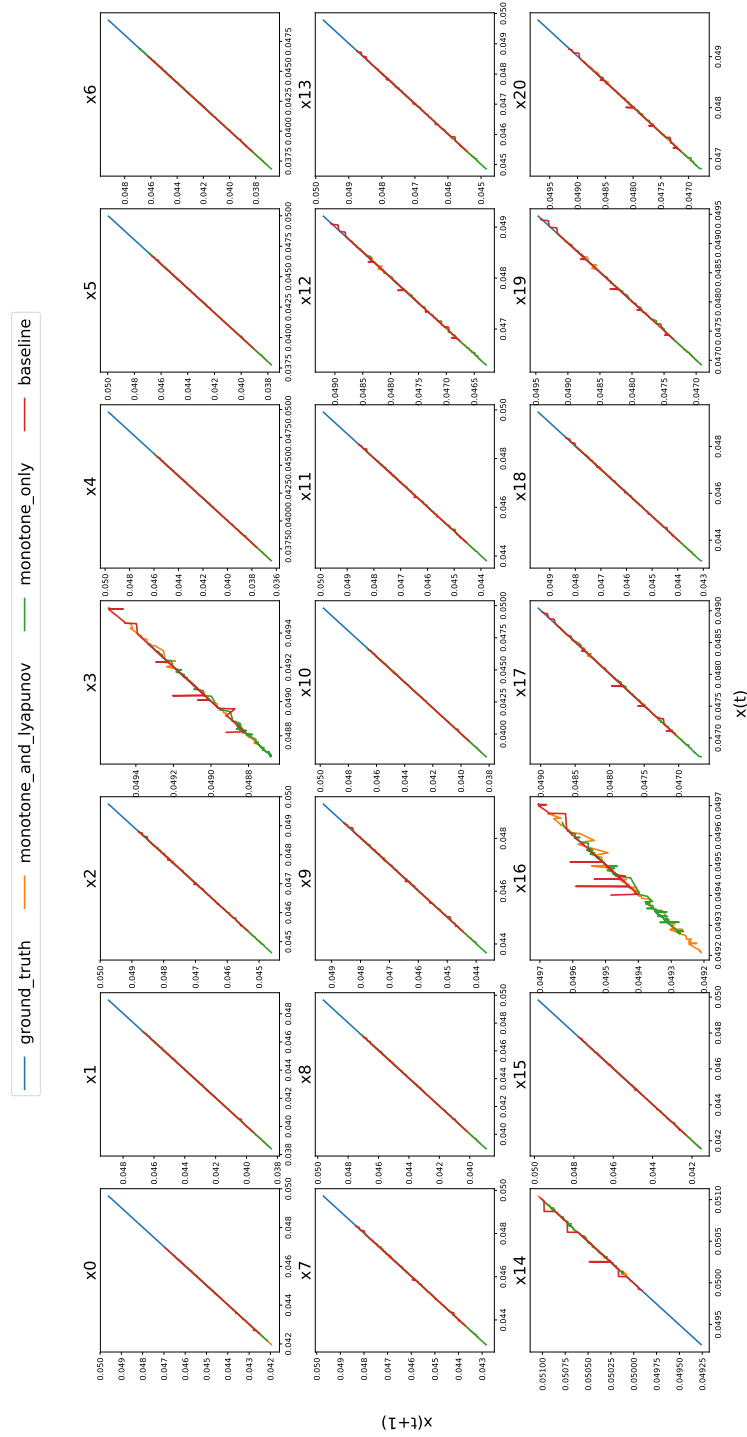


Figure 11: The $x(t+1)-x(t)$ relation of the predicted BCC model trajectory up to 250 time steps using 100-window.

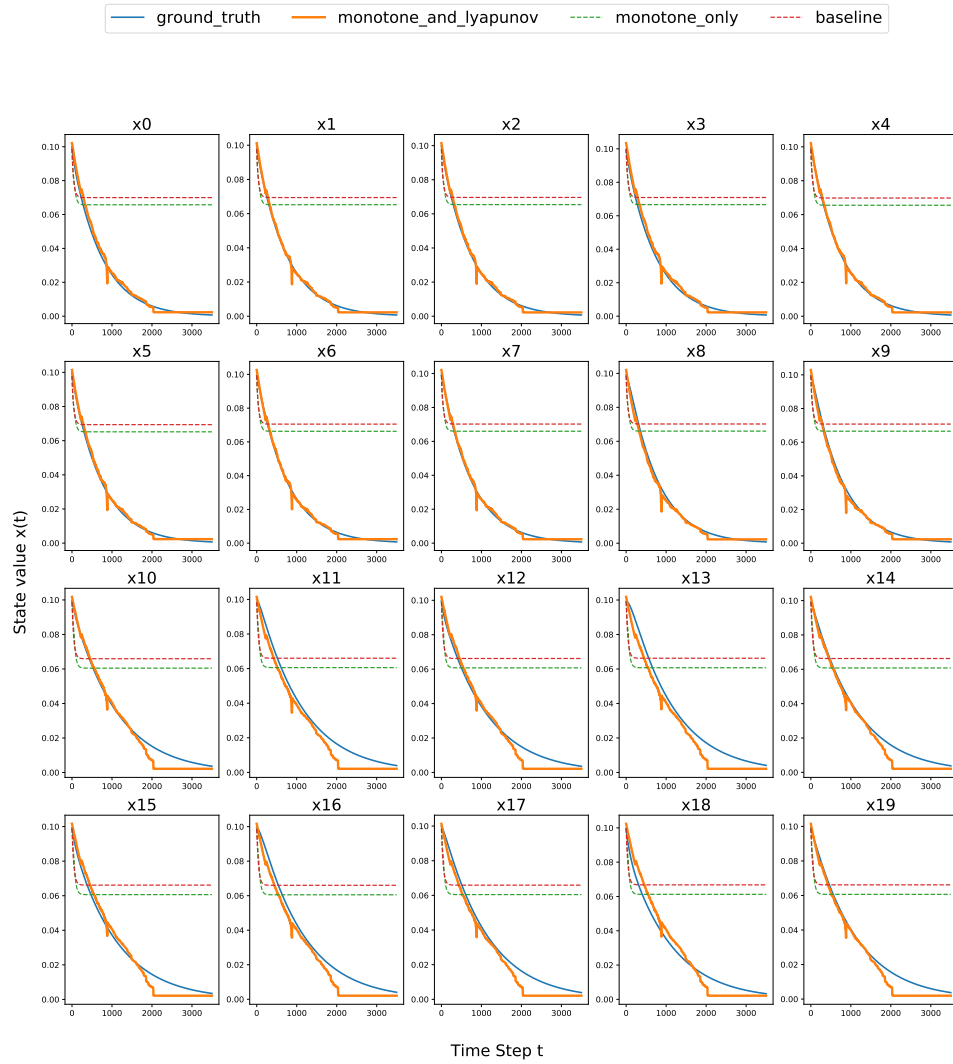


Figure 12: Predicted trajectories of the LV model using 1-window up to 3500 time steps

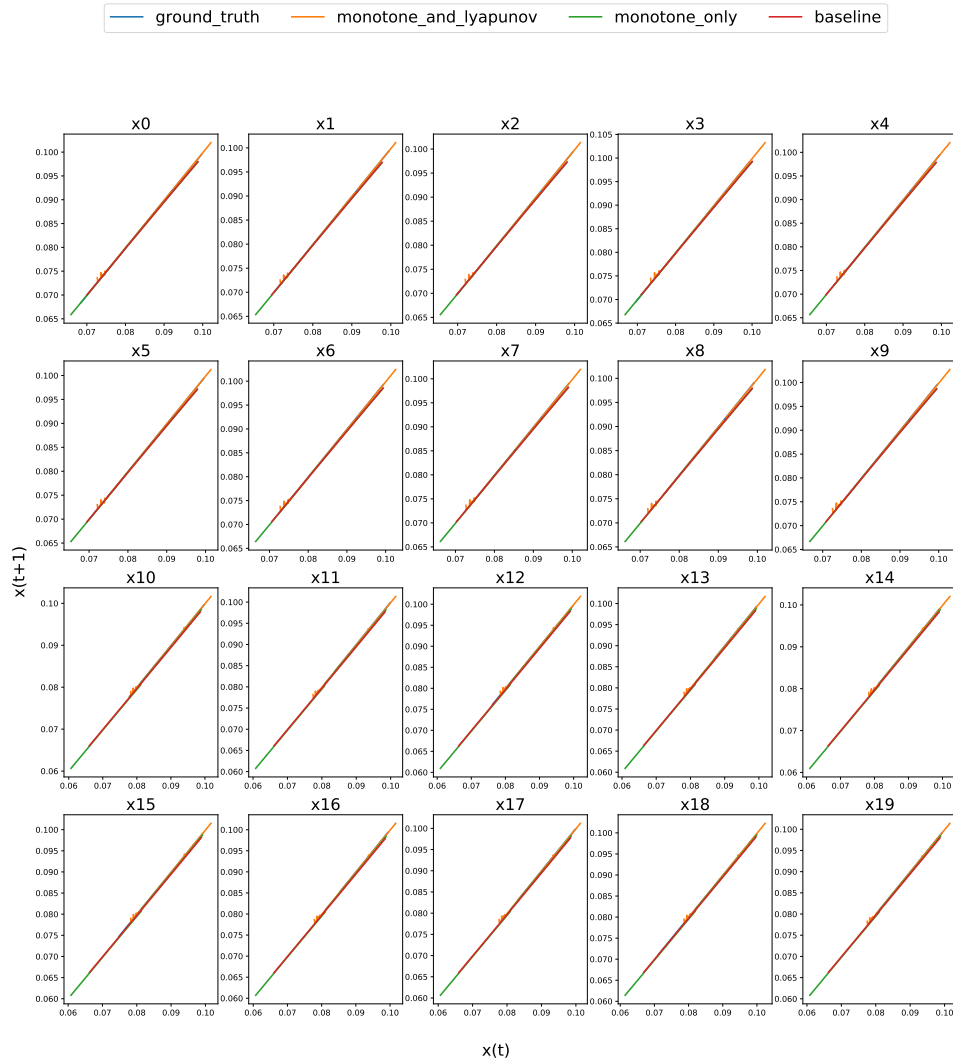


Figure 13: The $x(t+1)-x(t)$ relation of the predicted LV model trajectory up to 250 time steps using 1-window.

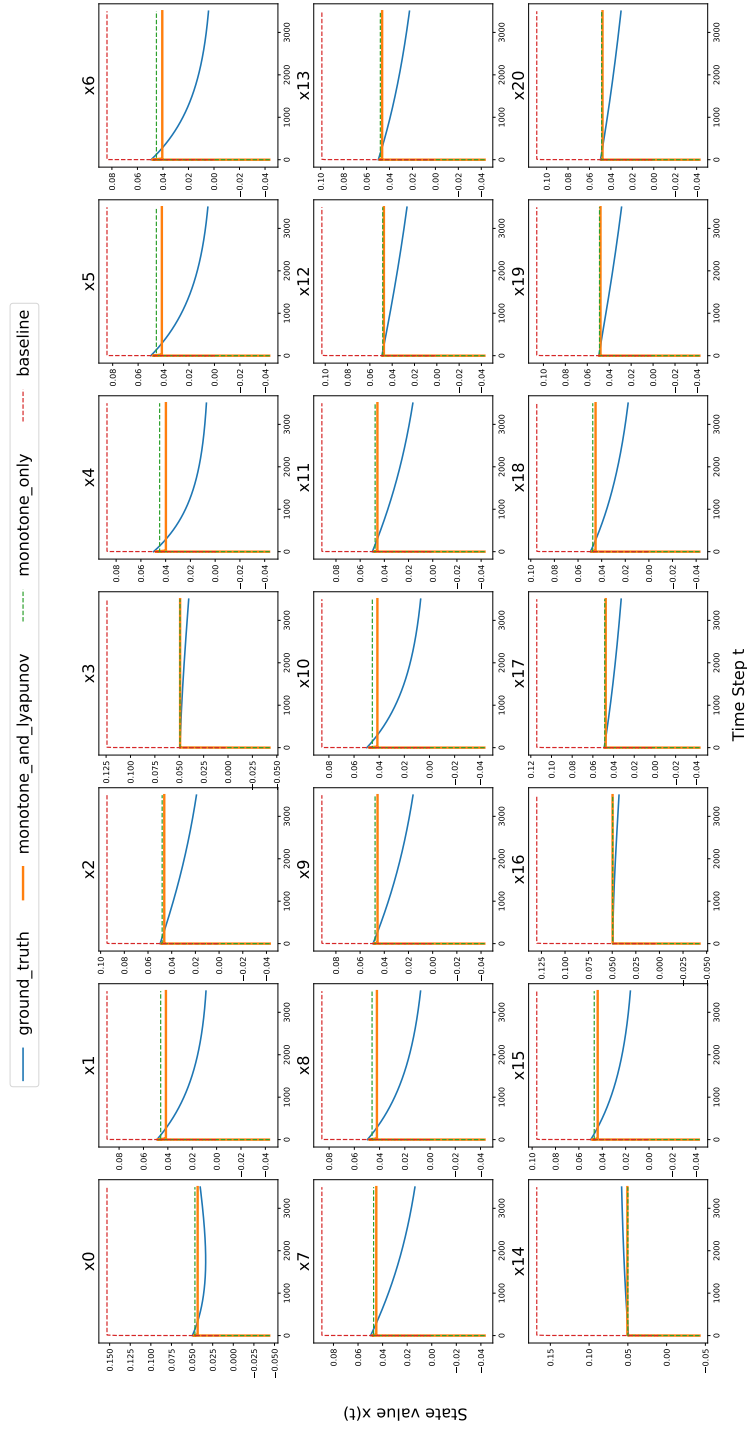


Figure 14: Predicted trajectories of the BCC model using 1-window up to 3500 time steps

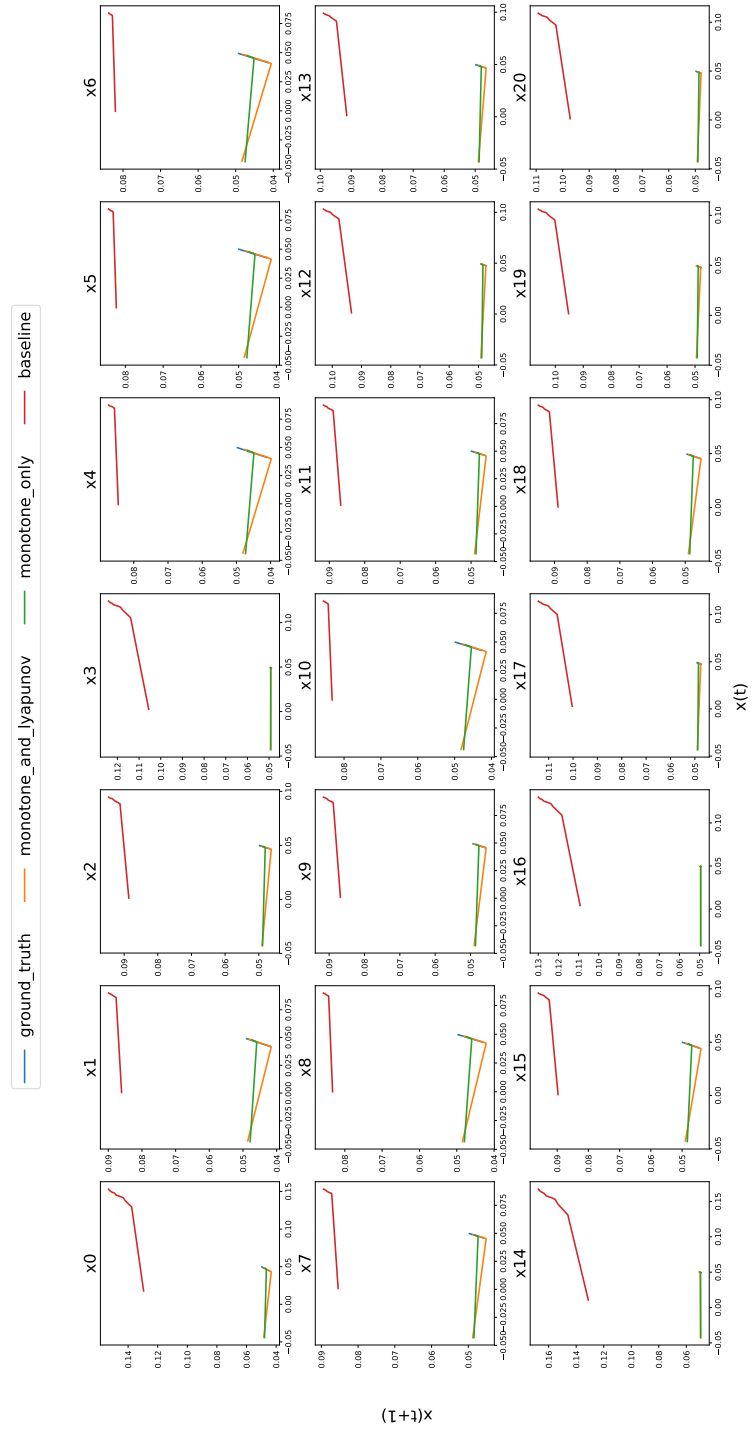


Figure 15: The $x(t + 1)$ - $x(t)$ relation of the predicted BCC model trajectory up to 250 time steps using 1-window.

E Algorithms

Algorithm 1 Predict $x(t + T)$ recursively using \mathcal{F}_θ with q -window

Input: $x(t : t - q + 1)$, p_i , $\mathcal{F}_\theta = \{\hat{f}_{\theta_i} | i \in [1, q]\}$, T

- 1:
- 2: **function** PRED($y_1, y_2, \dots, y_q, d, T$)
- 3: **if** $d == T$ **then**
- 4: **return** $\sum_{i=1}^q p_i \hat{f}_{\theta_i}(y_i)$
- 5: **else**
- 6: **return** PRED($y_2, y_3, \dots, \sum_{i=1}^q p_i \hat{f}_{\theta_i}(y_i), d + 1, T$)
- 7:

Main:

- 8: **return** PRED($x(t), x(t - 1), \dots, x(t - q + 1), 1, T$)

Algorithm 2 Predict $x(t + T)$ recursively using meta-NN \hat{f}_θ with q -window

Input: $x(t : t - q + 1)$, p_i , the meta-NN \hat{f}_θ , T

- 1:
- 2: **function** PRED($y_1, y_2, \dots, y_q, d, T$)
- 3: **if** $d == T$ **then**
- 4: **return** $\hat{f}_\theta(y_i)$
- 5: **else**
- 6: **return** PRED($y_2, y_3, \dots, \hat{f}_\theta(y_i), d + 1, T$)
- 7:

Main:

- 8: **return** PRED($x(t), x(t - 1), \dots, x(t - q + 1), 1, T$)
